Cell fate decision mediated by p53 pulses

Xiao-Peng Zhang, Feng Liu[1], Zhang Cheng, and Wei Wang[1]

National Laboratory of Solid State Microstructure and Department of Physics, Nanjing University, Nanjing 210093, China

Edited by Peter G. Wolynes, University of California at San Diego, La Jolla, CA, and approved June 4, 2009 (received for review December 23, 2008)

The tumor suppressor p53 plays a crucial role in cellular response to various stresses. Recent experiments have shown that p53 level exhibits a series of pulses after DNA damage caused by ionizing radiation (IR). However, how the p53 pulses govern cell survival and death remains unclear. Here, we develop an integrated model with four modules for the p53 network and explore the mechanism for cell fate decision based on the dynamics of the network. By numerical simulations, the following processes are characterized. First, DNA repair proteins bind to IR-induced double-strand breaks, forming complexes, which are then detected by ataxia telangiectasia mutated (ATM). Activated ATM initiates the p53 oscillator to produce pulses. Consequently, the target genes of p53 are selectively induced to control cell fate. We propose that p53 promotes the repair of minor DNA damage but suppresses the repair of severe damage. We demonstrate that cell fate is determined by the number of p53 pulses relying on the extent of DNA damage. At low damage levels, few p53 pulses evoke cell cycle arrest by inducing p21 and promote cell survival, whereas at high damage levels, sustained p53 pulses trigger apoptosis by inducing p53AIP1. We find that p53 can effectively maintain genomic integrity by regulating the efficiency and fidelity of DNA repair. We also show that stochasticity in the generation and repair of DNA damage leads to variability in cell fate. These findings are consistent with experimental observations and advance our understanding of the dynamics and functions of the p53 network.

p53 network | DNA repair | apoptosis | variability

The tumor suppressor protein p53 is a key mediator of cellular response to various stresses (1), and it performs its function primarily as a transcription factor, controlling the expression of a number of target genes (2). In response to DNA damage, the p53 signaling network is activated to induce cell cycle arrest, DNA repair, and apoptosis (1). Previously, it was proposed that p53 responds to DNA damage in an analog mode, i.e., a low level of p53 promotes cell survival by inducing cell cycle arrest and facilitating DNA repair, whereas a high level of p53 induces apoptosis to destroy irreparably damaged cells (1). Recently, damped oscillations of p53 level have been observed upon IR at the population level in several human cell lines and transgenic mice (3–6), with the amplitude of oscillations depending on the IR dose (5). More interestingly, pulses of p53 level were revealed in individual MCF7 cells, and the mean number of pulses, rather than the amplitude, was found to be related to the IR dose (7). This was suggested as a digital mode of p53 response (7). Later, it was further found that some MCF7 cells exhibit permanent p53 pulses whereas a few cells still show a finite number of p53 pulses during long-term observations (8). Such permanent oscillations may be related to the deficiency in DNA repair and apoptosis induction in those transformed cells (9–11). Moreover, the damped oscillations observed in cell populations can be interpreted as a summation of p53 pulses of individual cells (8, 12). Thus, the above experimental observations clearly justify the presence of p53 pulses at the single-cell level. An issue then arises concerning how the p53 pulses govern cell fate decision between survival and death after DNA damage. It is also intriguing to explore the relationship between p53 pulses and IR dose in untransformed cells.

Because IR is one of the most frequently used techniques in cancer therapy, it is of great significance to investigate the response of p53 signaling network to IR-induced DNA damage. Previously, several models have been proposed to elucidate the generation of p53 oscillations (3, 8, 12–15). Especially, Ma et al. (12) constructed a three-module model and found that p53 pulses can be generated based on a negative-feedback loop between p53 and Mdm2 with a long time delay. Zhang et al. (15) further proposed four dual-feedback mechanisms for p53 digital oscillations and classified the p53 pulses into three forms to explore the functions of p53. Most recently, Batchelor et al. (16) reported a recurrent mechanism for the generation of p53 pulses by ATM pulses. However, to obtain a coherent picture of the p53-mediated cellular response to DNA damage, several important aspects need be considered. First, both the generation of p53 pulses and cell fate decision should be included in modeling. Second, the functions of p53 pulses should be further elucidated. Third, the variability between individual cells in p53 dynamics should be reflected in the variability in cell fate. Fourth, because p53 also plays a transcription-independent role in DNA repair (17), the link between p53-mediated regulation of the repair process and cell fate decision should be built. These are important for the clarification of how p53 dynamically controls cell survival and death after DNA damage.

Here, we build an integrated model for the p53 signaling network and study the whole process from generation of DNA damage to cell fate decision. The model is composed of four subsystems: a DNA repair module, an ATM switch, the p53–Mdm2 oscillator, and a cell fate decision module. We propose that p53 plays a dual, transcription-independent role in DNA repair, i.e., p53 promotes the repair of minor DNA damage but suppresses the repair of severe damage. The combined negative and positive feedback loops between p53 and Mdm2 are responsible for robust oscillatory dynamics. We find that cell fate is governed by the number of p53 pulses, i.e., few pulses promote cell survival, whereas sustained pulses induce apoptosis. We show that p53 subserves the maintenance of genomic integrity by regulating the fidelity and efficiency of DSB repair. These findings advance our understanding of the dynamics and functions of the p53 network and provide clues for therapeutic manipulation of the p53 pathway in the treatment of cancer. Our work presents a theoretical framework for further exploring cellular response to stress.

Model

p53 Signaling Network with Four Modules. In this work, the p53 network is composed of four modules (Fig. 1). When cells are exposed to IR, a certain number of DSBs are first generated in every cell. With DNA repair proteins binding to the DSBs, DSB repair-protein complexes (DSBCs) form and the repair process ensues in the DNA repair module. Subsequently, ATM is activated by the DSBCs in the ATM switch module. Then p53 is activated by

Author Contributions: X.-P.Z., F.L., Z.C., and W.W. designed research; X-P.Z. performed research; X.-P.Z., F.L., Z.C., and W.W. analyzed data; and X.-P.Z., F.L., and W.W. wrote the paper.

The authors declare no conflict of interest.

This article is a PNAS Direct Submission.

Freely available online through the PNAS open access option.

[1]To whom correspondence may be addressed. E-mail: fliu@nju.edu.cn or wangwei@nju.edu.cn.

This article contains supporting information online at www.pnas.org/cgi/content/full/0813088106/DCSupplemental.

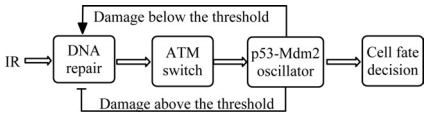

Fig. 1. An integrated model of p53 signaling network. There are four modules: a DNA repair module, an ATM switch, the p53–Mdm2 oscillator, and a cell fate decision module. The p53 regulation of DNA repair is threshold-dependent and is denoted as feedback from the p53–Mdm2 oscillator to the DNA repair module.

the active ATM, and the p53 level exhibits a series of pulses in the p53–Mdm2 oscillator module. Finally, in the cell fate decision module, p53 controls the expression of the target genes; cell cycle arrest and apoptosis are separately evoked by the induction of p21 and p53AIP1. Thus, the damage signal is transmitted forward until DNA repair is completed or apoptosis is initiated. In our model, it is assumed that p53 promotes repair when DNA damage is minor and suppresses it otherwise (Fig. 1). The details of each module are described in the following.

DNA Repair. The DNA repair module characterizes the generation and repair of IR-induced DSBs. For each cell, DSBs are first generated relying on the IR dose, D_{IR}, and the numbers of DSBs for a population obey a Poisson distribution with a mean of 35 $Gy^{-1} \times D_{IR}$ (18). The repair process then involves binding of repair proteins to the DSBs and releasing of the proteins from the fixed DSBs. Such a process proceeds in a stochastic way (see *SI Appendix* for details). Each locus in which a DSB is initially generated can be in one of three states corresponding to intact DSB, DSBC, and fixed DSB. Thus, the number of DSBs in each state can be used to describe the repair process. In the simulation, we adopt the two-lesion-kinetic model (19) (Fig. S1 and Eqs. 1–3 in *SI Appendix*) and characterize the dynamics of DSB repair by using a Monte Carlo method proposed by Ma et al. (12).

Generally, DSBs are repaired mainly by nonhomologous end-joining (NHEJ) in mammalian cells, especially in G_1 phase of the cell cycle (20). Note that p53 plays an important role in DNA repair (17). However, the effect of p53 on NHEJ is complicated: a stimulatory effect was observed (21, 22), whereas an inhibitory effect was also reported (23, 24). To reconcile these findings, it was speculated that p53 may inhibit error-prone repair but promote error-free repair (17). Thus, p53 regulates the fidelity of DSB repair. It was also shown that the fidelity is related to the number of DSBs, i.e., the fidelity is high or low for few and excessive DSBs, respectively (25, 26). Therefore, we assume that p53 promotes the DSB repair when the initial number of DSBs is below a threshold and suppresses it otherwise (Fig. 1). In the model, the threshold for DSB repair is set to 175, i.e., the mean number of DSBs generated at $D_{IR} = 5$ Gy.

ATM Switch. The ATM switch acts as a detector for DSBs, involving three components: ATM dimer (ATM_2), inactive ATM monomer (ATM), and active ATM monomer (ATM*) (Fig. S2 in *SI Appendix*). ATM exists predominantly as dimers in unstressed cells. After IR, DSBCs promote the conversion of inactive monomers to active ones, and a positive feedback further accelerates the activation of ATM through intermolecular autophosphorylation (27). Consequently, active monomers become dominant after IR.

In our model, the total concentration of ATM is assumed to be constant, and the rate of ATM activation is a function of the amounts of DSBC and ATM*. After IR, the concentration of ATM* rises from a low level to a high one; it returns to the low level when the number of DSBs becomes sufficiently small because of DNA repair. This behavior is characterized by a bistable switch with discrete "on" and "off" states. The switch transmits a switching signal to the downstream p53–Mdm2 oscillator, ensuring that it is initiated in an "all-or-none" manner. The "off" state of the switch leads to a low p53 level, whereas the "on" state drives a series of p53 pulses. The dynamics of the ATM switch are described by Eqs. 4–6 in *SI Appendix*.

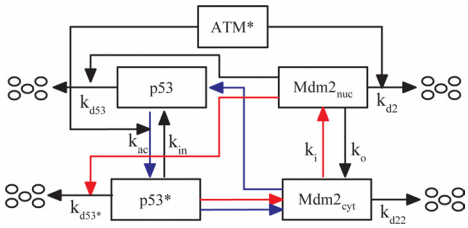

Fig. 2. Model of the p53–Mdm2 oscillator. Two forms of p53 in the nucleus are considered, inactive p53 and active p53*. Mdm2 in the nucleus and cytoplasm is denoted as $Mdm2_{nuc}$ and $Mdm2_{cyt}$, respectively. They can shuttle between the two compartments at rates k_i and k_o. Inactive p53 is degraded rapidly by Mdm2 at a rate k_{d53}, whereas active p53* is degraded slowly at a rate k_{d53*} because of its weak binding affinity to $Mdm2_{nuc}$. Combined negative (red lines) and positive (blue lines) feedback loops are responsible for p53 oscillations. In the negative-feedback loop, p53* promotes production of $Mdm2_{cyt}$, which then enters the nucleus to induce degradation of p53*. In the positive-feedback loop, p53* induces *Mdm2* to synthesize $Mdm2_{cyt}$, which promotes the translation of *p53* mRNA to produce inactive p53.

p53–Mdm2 Oscillator. The p53–Mdm2 oscillator generates pulses after the activation of ATM. This module is composed of two core proteins: p53 and its negative regulator, Mdm2 (Fig. 2). Here, only nuclear p53 is considered, whereas Mdm2 is classified into nuclear and cytoplasmic forms. In the nucleus, p53 is activated by ATM* in two ways: ATM* promotes the phosphorylation of p53 on Ser-15 (28) and accelerates the degradation of Mdm2 through phosphorylation (29). Thus, ATM* induces a conversion of p53 from the inactive state to the active state (p53*) (29). Meanwhile, p53* is deactivated at a basal rate. Here, only p53* can induce production of $Mdm2_{cyt}$, which promotes translation of *p53* mRNA in the cytoplasm (30). For simplicity, we assume that both the degradation rate of Mdm2 and the activation rate of p53 increase linearly with ATM* level (Eqs. 7–8 in *SI Appendix*).

Two coupled feedback loops are involved in the p53–Mdm2 oscillator. One is the negative-feedback loop between p53* and $Mdm2_{nuc}$ (the red lines in Fig. 2); the other is the positive one between p53* and $Mdm2_{cyt}$ (30) (the blue lines). In undamaged cells, p53 levels are kept low by Mdm2. After DNA damage, the p53–Mdm2 complex is dissociated because of activation of p53 by ATM*, with the negative feedback weakened. The levels of p53, p53*, and $Mdm2_{cyt}$ increase abruptly through the positive feedback. Subsequently, high-level $Mdm2_{nuc}$ enables the negative feedback to predominate again, and then p53 is degraded quickly. The alternate domination of the positive and the negative feedback can make p53 and Mdm2 levels oscillate periodically. Note that several theoretical studies have demonstrated that interlinked feedback loops are superior to a single feedback loop in response to various signals (14, 31, 32). It was argued that robust p53 oscillations can be accomplished through a combination of negative and positive feedback loops rather than a single negative feedback loop with a time delay (14, 32). The dynamics of this module are characterized by Eqs. 7–14 in *SI Appendix*.

Cell Fate Decision. In this module, p53 coordinates cell cycle arrest and apoptosis to govern cell fate, in which the phosphorylation of p53 at distinct sites is a key factor. For example, the primary phosphorylation of p53 on Ser-15 leads to cell cycle arrest, whereas its further phosphorylation on Ser-46 promotes expression of pro-apoptotic genes such as *p53AIP1* (33). Here, the above two forms of phosphorylated p53 are called p53 arrester and p53 killer, respectively (Fig. 3). Moreover, the product of p53 arrester-inducible gene *p53DINP1* contributes to the formation of p53 killer

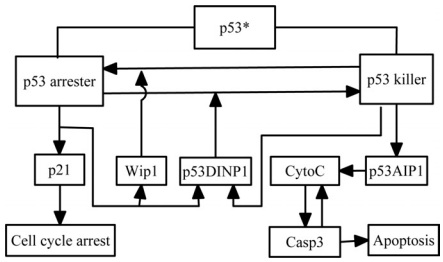

Fig. 3. Model of cell fate decision. There are two forms of active p53: p53 arrester and p53 killer. p53 arrester regulates the expression of *Wip1*, *p53DINP1*, and *p21*, whereas p53 killer controls the expression of *p53DINP1* and *p53AIP1*. CytoC and Casp3 are the pro-apoptotic components. There is a positive-feedback loop between CytoC and Casp3, which creates an apoptotic switch. The release of CytoC leads to activation of Casp3, which in turn cleaves the inhibitors of p53AIP1 (such as Bcl-2 and Bcl-xL) to enhance the release of CytoC.

(34), whereas that of another p53 arrester-inducible gene *Wip1* promotes the reversion of p53 killer to p53 arrester (35). Clearly, p53 arrester and p53 killer play distinct roles in cell fate decision. p53 arrester induces cell cycle arrest through the transcriptional activation of *p21*. Differently, p53 killer promotes the expression of pro-apoptotic genes such as *p53AIP1*. Over-expression of *p53AIP1* then induces the release of cytochrome *c* (CytoC) from mitochondrial caused by dissipation of mitochondrial membrane potential $\Delta\psi_m$ (33), and apoptosis rapidly ensues after the activation of Caspase 3 (Casp3). A positive-feedback loop between CytoC and Casp3 (36) underlies the apoptotic switch in our model (37). The dynamics of this module are described by Eqs. 15–22 in *SI Appendix*.

Results

An Overview of Signal Transduction in the p53 Network. Fig. 4 shows two examples of the output of each module after IR. The number of DSBCs, n_C, first rises rapidly to its maximum (here 20 DNA repair proteins per cell is assumed). Then DSBCs turn on the ATM switch, and the activated ATM initiates the p53–Mdm2 oscillator to produce p53 pulses. The number of p53 pulses is determined by the duration of ATM in the activated state. At the low IR dose of 3 Gy, transient p53 pulses cannot activate Casp3, and the cell recovers to normal growth after the damage is effectively repaired (Fig. 4*A*). At the high dose of 5 Gy, sustained p53 pulses lead to apoptosis through activation of Casp3 (Fig. 4*B*). This means that minor DNA damage only evokes protective cell cycle arrest and severe damage induces apoptosis. It is found that cell fate is governed by the number of p53 pulses, n_P. In our model, when $n_P < 6$, slightly damaged cells recover to normal growth; when $n_P \geq 6$, the

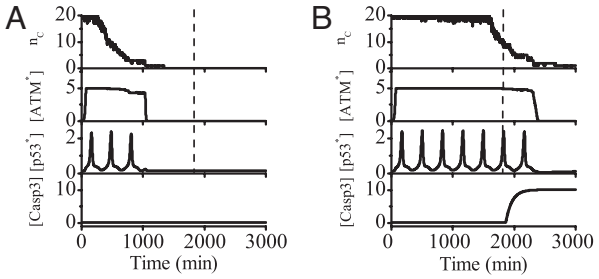

Fig. 4. Overview of signal transduction in the p53 network. Shown are time courses of the output of each module at the IR dose of 3 Gy (*A*) or 5 Gy (*B*). Upon IR, a number of DSBCs, n_C, are produced and then ATM is activated, initiating the p53 oscillations. When DNA damage is effectively repaired, the ATM switch is turned off and the concentration of p53* returns to a low level. At low IR doses, few p53 pulses cannot activate Casp3 and the cell recovers to normal growth. At high doses, sustained p53 pulses lead to activation of Casp3 and apoptosis ensues. The dashed lines denote a threshold time for cell fate decision.

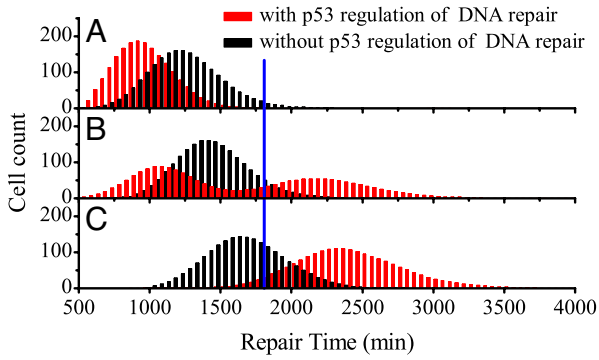

Fig. 5. Histograms of repair time. The cell count vs. the repair time is plotted for a population of 2,000 cells with and without p53 regulation (red and black lines, respectively) at the IR dose of 4 Gy (*A*), 5 Gy (*B*), or 6 Gy (*C*). The blue line denotes the threshold time for cell fate decision. With p53 regulation, the repair process depends on the levels of p53 and DNA damage, i.e., p53 promotes the repair of minor damage but suppresses the repair of severe damage. A threshold of 175 DSBs is set to distinguish between low and high damage levels.

concentration of p53AIP1 gradually accumulates to a high level and oscillates there until Casp3 level exceeds a threshold for apoptosis induction (see Fig. S11 in *SI Appendix*). That is, the critical pulse number for cell fate decision is 6. Note that such a value depends on the model and the parameter set. The dashed lines in Fig. 4 denote the threshold time taken for the number of p53 pulses to reach the critical number, i.e., cells recover to normal proliferation if DSB repair is finished before that time and otherwise are eliminated through apoptosis.

DNA Damage Repair. Because of stochasticity in the initial numbers of DSBs and repair dynamics, individual cells under identical conditions show considerable variability in the repair time, which is defined as the time taken for the number of DSBs to reduce below 2 (here the apoptotic effect is not involved). A histogram of the repair time for 2,000 cells is used to characterize the variability in repair time. In the presence of p53 regulation of DNA repair, the histograms are unimodal at low and high IR doses (Fig. 5 *A* and *C*), whereas the histogram becomes bimodal around $D_{IR} = 5$ Gy (Fig. 5*B*). The mean repair time increases with IR dose, and the histogram moves rightward for higher dose (see Figs. S3 and S4 in *SI Appendix* for details). In the absence of p53 regulation, however, the histograms are all unimodal at various IR doses.

Note that p53 regulates the efficiency of DNA repair in a threshold-dependent manner: p53 promotes the repair when the initial number of DSBs is less than 175 and suppresses the repair otherwise. At low IR doses, say $D_{IR} = 4$ Gy, p53 promotes the repair with high fidelity, and the histogram for the case with p53 regulation shifts leftward (Fig. 5*A*). At high doses, say $D_{IR} = 6$ Gy, p53 represses the repair, and the histogram for the case with p53 regulation shifts rightward (Fig. 5*C*). Interestingly, at $D_{IR} = 5$ Gy, the repair time for some cells decreases whereas that for the others increases, compared with the case without p53 regulation. As a result, the histogram becomes bimodal.

The histogram for the case without p53 regulation at $D_{IR} = 5$ Gy is consistent with that in figure 5*C* in ref. 12. Differently, here the dual role of p53 in regulation of DNA repair has significant implications for the maintenance of genomic integrity. Because the repair of slight damage is strengthened and that of severe damage is repressed, p53 promotes the repair with high fidelity and suppresses the repair with low fidelity. As we shall see later, this is in concert with the role of p53 in cell fate decision, i.e., p53 promotes survival of reparably damaged cells or apoptosis of irreparably damaged cells. Therefore, DNA repair and cell fate decision are well coordinated by p53.

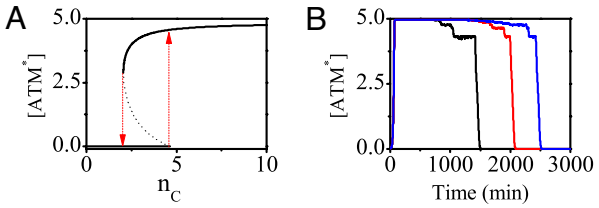

Fig. 6. Switching behavior of ATM. (*A*) Bifurcation diagram of ATM* level vs. the number of DSBCs, n_C. The ATM switch turns on if $n_C > 4$ (the upward arrow) or turns off if $n_C < 3$ (downward arrow). (*B*) Time courses of ATM* level for 3 individual cells at D_{IR} = 5 Gy. The ATM switch is on during the DSB repair process and is off only after DSBs are effectively repaired.

ATM Switch. As a detector for DSBs, the activation of ATM exhibits a switch-like behavior (Fig. 6 and Fig. S5 in *SI Appendix*). Because n_C varies on a time scale of hours but ATM equilibrates in minutes because of fast phosphorylation (Fig. 4), ATM* level follows the time course of n_C adiabatically. The steady-state ATM* level versus n_C is plotted in Fig. 6*A*. ATM activation starts with $n_C = 5$, whereas ATM deactivation occurs when $n_C = 2$ (i.e., the DNA damage is effectively repaired). Thus, ATM* level indeed behaves as a bistable switch, with the on (off) state corresponding to the upper (lower) branch in Fig. 6*A*.

The time courses of ATM* level for 3 individual cells at D_{IR} = 5 Gy are plotted in Fig. 6*B* (see also Fig. S6 in *SI Appendix*). After IR, ATM is activated rapidly and its level reaches a high plateau with [ATM*] ≈ 5. The width of the plateau is distinct for different cells, showing considerable variability. Besides that plateau, there exist two short lower plateaus separately corresponding to $n_C = 4$ and $n_C = 3$. Clearly, the duration of active ATM state is determined by the repair time and prolongs with increased IR dose (Fig. 4 and Fig. S6 in *SI Appendix*). Moreover, once $n_C < 3$, ATM* level decays to zero quickly. This step-like response results from the positive feedback involved in the autophosphorylation of ATM (27). These results indicate that few DSBs are able to activate ATM rapidly and ATM remains active until DNA damage is effectively repaired. Therefore, ATM is a sensitive and reliable detector for DSBs. Furthermore, the ATM* activity relays an on–off switching signal to the p53–Mdm2 oscillator.

p53 Pulses. The generation of p53 pulses is controlled by active ATM. To show this, a bifurcation diagram of p53* level versus ATM* level is plotted in Fig. 7*A*. When [ATM*] < 0.7, p53 remains at a low level. There is a Hopf bifurcation (labeled as "HB") at [ATM*] = 0.7, and beyond that p53* level undergoes periodical oscillations. As seen in Figs. 7*A* and 6*A*, the on state of ATM* evokes the p53 oscillations, whereas the off state terminates them. Thus, ATM* level is limited in a region between 2.9 and 5.0 for driving p53 oscillations.

Fig. 7*B* shows the time evolution of four components of the p53–Mdm2 oscillator, describing the generation of the pulses. After IR, p53* level rises abruptly owing to activation by ATM*. In contrast, $Mdm2_{nuc}$ level first decreases because of its accelerated degradation induced by ATM* and then increases after the rise of $Mdm2_{cyt}$ because of p53 induction. As a result, the translation rate of *p53* mRNA rises, leading to a further increase in p53* level. Meanwhile, more $Mdm2_{cyt}$ enters the nucleus, and the p53* level drops when $Mdm2_{nuc}$ level is high enough. Subsequently, Mdm2 levels fall because of a reduction in synthesis. Thus, p53* level exhibits the pulse-like behavior. The oscillation period (≈5.5 h) and phase differences between components are in agreement with the experimental observations (8). Moreover, the parameter dependence of the period and amplitude of p53 oscillations is presented in Figs. S7 and S8 in *SI Appendix*.

Fig. 7*C* shows the time courses of p53* level for 3 cells at D_{IR} = 5 Gy. The amplitudes and periods of p53 pulses are almost constant.

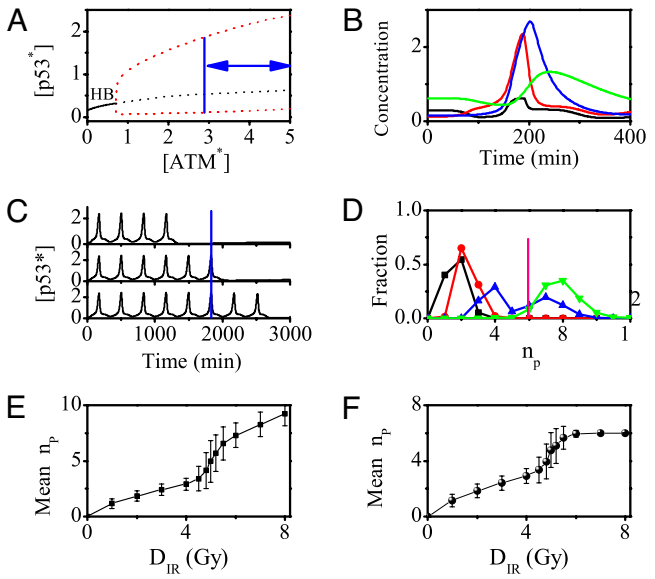

Fig. 7. p53 pulses. (*A*) Bifurcation diagram of p53* level vs. ATM* level. In unstressed cells, ATM is inactive and p53 remains in a low-level steady state (solid line). Upon IR, the steady state becomes unstable (black dashed line), and p53* level undergoes oscillations between the maxima and minima of the limit cycle (red dashed lines) when ATM level is in the region marked by the bidirectional arrows. (*B*) Time course of the levels of p53 (black), p53* (red), $Mdm2_{cyt}$ (blue), and $Mdm2_{nuc}$ (green) over one period. (*C*) A series of p53 pulses for three individual cells at D_{IR} = 5 Gy. The blue line denotes the threshold time for cell fate decision (compare Fig. 4). (*D*) Fraction of cells with different numbers of pulses at IR doses of 1 Gy (black), 3 Gy (red), 5 Gy (blue), and 6 Gy (green). The pink line denotes the critical pulse number for cell fate decision. (*E*) The mean n_P vs. D_{IR} without the effect of apoptosis. (*F*) The mean n_P vs. D_{IR} with the effect of apoptosis. Here the mean number is obtained by averaging over 2,000 cells, and the error bars indicate the standard deviation.

However, the numbers of p53 pulses are variable because of the stochasticity in the generation and repair of DSBs as shown in Fig. 5. Sparse p53 pulses cease when DNA damage is quickly repaired; when the DSBs cannot be fixed within the threshold time, p53 pulses persist until apoptosis is induced. Moreover, the averaged p53* level over 2,000 individual cells exhibits damped oscillations (Fig. S9 in *SI Appendix*), consistent with the experimental observation (3). Note that if the cells are deficient in apoptosis induction and DNA repair, the p53 pulses may last permanently as observed in MCF7 cells (8).

To show variability between cells in p53 dynamics, the histograms of the number of p53 pulses are plotted for four IR doses in Fig. 7*D*. It is seen that the number of p53 pulses shows considerable variability for certain D_{IR}, and most distributions are unimodal except a bimodal one for D_{IR} = 5 Gy. The distributions here are correlated with those of the repair time shown in Fig. 5. Furthermore, the mean n_P averaged over 2,000 cells versus D_{IR} is presented in Fig. 7 *E* and *F*. When the apoptotic effect is not involved, i.e., the pulses persist until all DNA damage is fixed, the mean n_P first increases linearly, then rapidly and finally linearly again with increasing D_{IR} (Fig. 7*E*). The two linear regions are related to the unimodal distributions in Fig. 7*D*. There is a large fluctuation in n_P around D_{IR} = 5 Gy because of the bimodal distribution in Fig. 7*D*. Differently, when the effect of apoptosis is included, the mean n_P becomes saturated at high D_{IR} (Fig. 7*F*). Clearly, this is because most cells commit suicide when $n_P = 6$. Taken together, a sigmoidal relationship between the mean pulse number and IR dose is found, and a digital mode of p53 response is presented.

Cell Fate Decision. p53 pulses govern cell fate through selective induction of the target genes. Fig. 8*A* shows the time courses of the

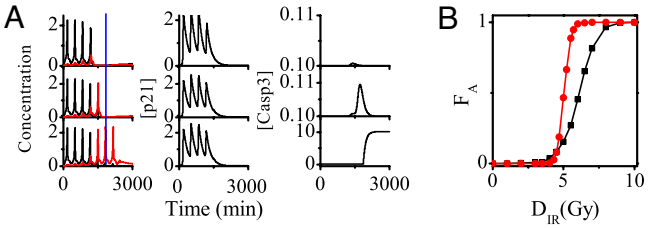

Fig. 8. p53-induced cell cycle arrest and apoptosis. (*A*) Time courses of the levels of p53 arrester and p53 killer (*Left*), p21 (*Center*), and Casp3 (*Right*) for 3 cells at the IR dose of 5 Gy. In *Left*, the blue line denotes the threshold time for cell fate decision and the black and red pulses represent p53 arrester and p53 killer, respectively. There exists remarkable variability in p53 dynamics and cell fate. (*B*) Fraction of apoptotic cells within a 2,000 cell population, F_A, vs. D_{IR} for the cases with (circles) and without (squares) p53 regulation of DNA repair.

levels of p53 arrester, p53 killer, p21, and Casp3 after IR. The first four p53 pulses consist of p53 arrester, whereas the fifth and subsequent pulses are composed of p53 killer. A conversion from p53 arrester to p53 killer occurs because of the accumulation of p53DINP1 induced by p53 arrester (Fig. 3). If DNA damage is quickly repaired, only pulses of p53 arrester appear and the cell cycle inhibitor p21 is produced (the first row in Fig. 8*A*). Consequently, the cell recovers to normal proliferation after a transient cell cycle arrest. In contrast, if DNA damage is severe, the pulses of p53 killer become dominant after those of p53 arrester, inducing p53AIP1. Subsequently, Casp3 level quickly rises to a high value and remains there thereafter, behaving as a bistable switch (see also Figs. S10 and S11 in *SI Appendix*), and finally apoptosis ensues (the third row in Fig. 8*A*). Interestingly, a reversion of apoptosis occurs at the early stage of its onset because of the DNA repair (the middle row in Fig. 8*A*), which is consistent with the experimental observation (38). This happens when DNA damage is effectively repaired before the pro-apoptotic components are fully activated. Therefore, the conversion between p53 arrester and killer links the extent of DNA damage with cell fate.

Given stochasticity in the generation and repair of DSBs, there exists variability in p53 dynamics and cell fate. To quantify such variability, the fraction of apoptotic cells in a population, F_A, versus D_{IR} is shown in Fig. 8*B*. Compared with the case without p53 regulation of DNA repair, F_A increasing with IR dose shows a switch-like behavior for the case with p53 regulation. This is because p53 promotes repair at low damage levels but suppresses it at high damage levels. Such a regulation can reduce cellular heterogeneity in cell fate, so that most cells either survive minor DNA damage or are destroyed because of severe damage. This may be important for cancer therapy (39). Thus, p53 can fine tune its regulation of DNA repair to maintain genomic integrity. These predictions can be tested by further experiments.

Discussion

Implications of p53 Pulses in Cell Fate Decision. As mentioned in the beginning of the paper, p53 pulses were observed in individual MCF7 cells (7, 8), whereas damped p53 oscillations were also observed in other cell lines (4), implying the presence of pulses at the single-cell level (12, 13). But these damped oscillations can be disrupted by high-level Mdm2 attributable to a single-nucleotide polymorphism in the *Mdm2* gene, together with the acceleration of tumor formation (4). These indicate that the pulsatile response of p53 is important in cellular response to DNA damage, as proposed by Lahav and coworkers (7).

Based on the presence of such p53 pulses, here we demonstrated how p53 pulses govern cell fate in putatively normal cells with intact DNA repair and apoptosis systems. We showed that the number of p53 pulses can be used to distinguish cell survival from apoptosis relying on the extent of DNA damage. We observed that there exists variability in the number of p53 pulses and the mean number has a sigmoidal relationship with the radiation dose. We found that the pulsatile response of p53 level enables the p53 network to repeatedly evaluate the damage signal and thus exerts a reliable and flexible control on cell fate decision. That is, p53 pulses can be terminated rapidly to avoid inappropriate death once DNA damage is effectively fixed, or apoptosis is triggered to maintain genomic integrity once the number of p53 pulses exceeds the critical number. Thus, our proposal that cell fate can be determined by counting the number of p53 pulses represents a reasonable mechanism.

Actually, there can exist considerable variability in the amplitudes of p53 pulses as shown experimentally (8). Providing that apoptosis is triggered when the levels of the pro-apoptotic factors are integrated over the cycles of p53 pulses to reach certain thresholds, the number of p53 pulses required for inducing apoptosis may depend on the amplitudes of p53 pulses. In this sense, cell fate decision is related to the amplitude of p53 level. In addition, as the mode of p53 response to DNA damage may be cell- and stress-type specific, different modes could be related to distinct mechanisms for cell fate decision. Clearly, our integrated model will be helpful to explore those mechanisms because the present framework describes a generic signaling pathway for the p53 response to stress, and each module can be separately and easily modified to accommodate new experimental observations.

p53 Pulses Act as a Molecular Timer. In our model, p53 pulses are classified into p53 arrester and p53 killer according to their distinct functions. The p53 pulses can be considered as a molecular timer for downstream events such as cell cycle arrest and apoptosis. Cell cycle arrest is induced by the transcriptional activation of *p21* during the first pulse of p53 arrester. That is, the first alarm of the timer is set for initiation of cell cycle arrest once DNA damage is produced. The cell cycle arrest persists during the pulses of p53 arrester. When DNA damage is severe, pulses of p53 killer gradually develop accompanying the pulses of p53 arrester. Thus, as the second alarm of the timer, the activation of p53 killer sends a warning signal for initiation of apoptosis, leading to expression of pro-apoptotic genes such as *p53AIP1*. Subsequently, the release of CytoC and activation of Casp3 lead to apoptosis. Note that, if the DNA repair is completed during the first pulse of p53 killer, the apoptotic alarm ceases and cells recover to normal proliferation.

Dual Role of p53 in DNA Repair. We propose that p53 promotes the repair of minor DNA damage but represses the repair of severe damage. This ensures that reparably damaged cells are protected from apoptosis and irreparably damaged cells are more prone to commit suicide. Therefore, the dual role of p53 in DNA repair is consistent with its function as a tumor suppressor, and this can also reconcile the controversy about the effect of p53 on NHEJ (17, 22, 24). It would be interesting to test these predictions in future experiments. In addition, given the stochasticity in DSB generation and repair dynamics, whether damaged cells survive or die becomes probabilistic, and the probability for apoptosis is determined by radiation dose. The p53 regulation of DNA repair makes cell fates more homogeneous at the population level. Specially, the pro-apoptotic function of p53 is enhanced at high damage levels, decreasing cellular heterogeneity. This may be important to radiation therapy for cancer (39).

ATM Dynamics. The p53 pulses can be evoked by ATM which shows a switch-like behavior as shown in this work and also in the previous work (12). This switch-like activation of ATM has been observed experimentally (27). Here, we further showed that the ATM switch, as a detector for DNA damage, is capable of initiating and terminating p53 oscillations. Once ATM is activated, the amplitude and period of p53 pulses are almost constant, guaranteeing an all-or-none response of p53 to DNA damage. There is only a feedforward connection between the ATM switch and downstream

p53 oscillator. However, the p53 pulses can also be evoked by the ATM pulses in the recurrent initiation mechanism reported recently (16). Meanwhile, the ATM activity is suppressed by p53 pulses but reactivated by DNA damage, depending on a negative feedback loop between ATM and p53 via Wip1. These results mean that robust p53 pulses can be triggered by both switch- and pulse-like ATM dynamics, and which mode is in action may be cell-type dependent. No matter how p53 pulses are generated, we believe, cell fate decision can still be governed by the pulses through selectively inducing downstream target genes, provided that ATM acts as a reliable detector for DNA damage.

Remarks on the Model. For simplicity, some other factors related to apoptosis, such as Bcl-2, Apaf-1, Bax, and Puma, are not involved in our model (40). Although these factors are important to the regulation of apoptosis under some conditions, there is no direct evidence that they are target genes of p53 killer. Moreover, constrained by available experimental data, we did not consider the intrinsic noise in gene expression. However, such noise may be important under some conditions. For example, nonadiabatic noise from binding and unbinding of proteins to DNA plays a key role in determining the region of the parameter space accommodating excitable behavior (41). Moreover, when the number of proteins involved in the gene network is very small, noise from extinction and resurrection of protein species can evoke bistability in the deterministically monostable system (42). It has also been demonstrated that potential energy landscape can be exploited to study the global features of cellular networks with intrinsic noise, such as stability and robustness (43–45). Presumably, adding intrinsic noise to our model will make the amplitude of p53 pulses more variable and result in more variability between individual cells in cell fate. Therefore, it would be intriguing to assess whether the proposed mechanism for cell fate decision is robust to noise.

Conclusion

The present work characterizes the whole process from generation of DNA damage to cell fate decision upon IR at the single-cell level. An integrated model with four modules has been proposed for the p53 network in response to DNA damage. The network exhibits rich dynamics: the switch-like activation of ATM, a series of discrete p53 pulses, and the apoptotic switch controlled by the pulses. It is shown that at low damage levels, few p53 pulses induce transient cell cycle arrest and augment DNA repair, whereas at high damage levels, sustained p53 pulses suppress DNA repair and induce apoptosis. This indicates a digital mode of p53 response. In addition, p53 can effectively maintain genomic integrity by regulating the efficiency and fidelity of DNA repair. Moreover, the stochasticity in DSB generation and repair dynamics is well responsible for the variability in cell fate. Our results are consistent with experimental observations, and our predictions are experimentally testable. The proposed theoretical framework can be used to further explore how the p53 network responds to stresses. Our work provides clues for designing more effective and less toxic treatments for cancer.

Materials and Methods

Details of the equations, parameter values, and methods for our model are presented in the *SI Appendix*. The stochastic DNA repair process was characterized by a Monte Carlo method. The units of time and radiation dose are minute and gray, respectively, and the other variables are dimensionless.

ACKNOWLEDGMENTS. We thank John J. Tyson, Galit Lahav, and Jun Wang for helpful comments on the manuscript. This work was supported by National Basic Research Program (China) Grants 2007CB814806 and 2006CB910302, NNSF (China) Grant 10834002, and NCET-08-0269.

1. Vousden KH, Lane DP (2007) p53 in health and disease. *Nat Rev Mol Cell Biol* 8:275–283.
2. Harris SL, Levine AJ (2005) The p53 pathway: positive and negative feedback loops. *Oncogene* 24:2899–2908.
3. Lev Bar-Or R, et al. (2000) Generation of oscillations by the p53-Mdm2 feedback loop: A theoretical and experimental study. *Proc Natl Acad Sci USA* 97:11250–11255.
4. Hu W, et al. (2007) A single nucleotide polymorphism in the Mdm2 gene disrupts the oscillation of p53 and Mdm2 levels in cells. *Cancer Res* 67:2757–2765.
5. Ramalingam S, et al. (2007) Quantitative assessment of the p53-Mdm2 feedback loop using protein lysate microarrays. *Cancer Res* 67:6247–6252.
6. Hamstra DA, et al. (2006) Real-time evaluation of p53 oscillatory behavior in vivo using bioluminescent imaging. *Cancer Res* 66:7482–7489.
7. Lahav G, et al. (2004) Dynamics of the p53-Mdm2 feedback loop in individual cells. *Nat Genet* 36:147–150.
8. Geva-Zatorsky N, et al. (2006) Oscillations and variability in the p53 system. *Mol Syst Biol* 2:2006.0033
9. Blanc C, et al. (2000) Caspase-3 is essential for procaspase-9 processing and cisplatin-induced apoptosis of MCF-7 breast cancer cells. *Cancer Res* 60:4386–4390.
10. Tyson JJ (2006) Another turn for p53. *Mol Syst Biol* 2:2006.0032.
11. Francisco DC, et al. (2008) Induction and processing of complex DNA damage in human breast cancer cells MCF-7 and nonmalignant MCF-10A cells. *Free Radic Biol Med* 44:558–569.
12. Ma L, et al. (2005) A plausible model for the digital response of p53 to DNA damage. *Proc Natl Acad Sci USA* 102:14266–14271.
13. Tiana G, Jensen MH, Sneppen K (2002) Time delay as a key to apoptosis induction in the p53 network. *Eur Phys J B* 29:135–140.
14. Ciliberto A, Novak B, Tyson JJ (2005) Steady states and oscillations in the p53/Mdm2 network. *Cell Cycle* 4:488–493.
15. Zhang T, Brazhnik P, Tyson JJ (2007) Exploring mechanisms of the DNA-damage response: p53 pulses and their possible relevance to apoptosis. *Cell Cycle* 6:85–94.
16. Batchelor E, Mock CS, Bhan I, Loewer A, Lahav G (2008) Recurrent initiation: a mechanism for triggering p53 pulses in response to DNA damage. *Mol Cell* 30:277–289.
17. Sengupta S, Harris CC (2005) p53: traffic cop at the crossroads of DNA repair and recombination. *Nat Rev Mol Cell Biol* 6:44–55.
18. Rothkamm K, Lobrich M (2003) Evidence for a lack of DNA double-strand break repair in human cells exposed to very low x-ray doses. *Proc Natl Acad Sci USA* 100:5057–5062.
19. Stewart RD (2001) Two-lesion kinetic model of double-strand break rejoining and cell killing. *Radiat Res* 156:365–378.
20. Burma S, Chen BPC, Chen DJ (2006) Role of non-homologous end joining (NHEJ) in maintaining genomic integrity. *DNA Repair* 5:1042–1048.
21. Yang T, et al. (1997) p53 induced by ionizing radiation mediates DNA end-joining activity, but not apoptosis of thyroid cells. *Oncogene* 14:1511–1519.
22. Tang W, Willers H, Powell SN (1999) p53 directly enhances rejoining of DNA double-strand breaks with cohesive ends in gamma-irradiated mouse fibroblasts. *Cancer Res* 59:2562–2565.
23. Bill CA, Yu Y, Miselis NR, Little JB, Nickoloff JA (1997) A role for p53 in DNA end rejoining by human cell extracts. *Mutat Res* 385:21–29.
24. Akyuz N, et al. (2002) DNA substrate dependence of p53-mediated regulation of double-strand break repair. *Mol Cell Biol* 22:6306–6317.
25. Jeggo PA (2002) The fidelity of repair of radiation damage. *Radiat Prot Dosimetry* 99:117–122.
26. Brady N, Gaymes TJ, Cheung M, Mufti GJ, Rassool FV (2003) Increased error-prone NHEJ activity in myeloid leukemias is associated with DNA damage at sites that recruit key nonhomologous end-joining proteins. *Cancer Res* 63:1798–1805.
27. Bakkenist CJ, Kastan MB (2003) DNA damage activates ATM through intermolecular autophosphorylation and dimer dissociation. *Nature* 421:499–506.
28. Prives C (1998) Signaling to p53: breaking the Mdm2–p53 circuit. *Cell* 95:5–8.
29. Stommel JM, Wahl GM (2004) Accelerated Mdm2 auto-degradation induced by DNA-damage kinases is required for p53 activation. *EMBO J* 23:1547–1556.
30. Yin Y, Stephen CW, Luciani MG, Fahraeus R (2002) p53 stability and activity is regulated by Mdm2-mediated induction of alternative p53 translation products. *Nat Cell Biol* 4:462–467
31. Zhang XP, Cheng Z, Liu F, Wang W (2007) Linking fast and slow positive feedback loops creates an optimal bistable switch in cell signaling. *Phys Rev E* 76:031924.
32. Pomerening JR, Kim SY, Ferrell JE Jr (2005) Systems-level dissection of the cell-cycle oscillator: bypassing positive feedback produces damped oscillations. *Cell* 122:565–578.
33. Oda K, et al. (2000) p53AIP1, a potential mediator of p53-dependent apoptosis, and its regulation by Ser-46-phosphorylated p53. *Cell* 102:849–862.
34. Okamura S, et al. (2001) p53DINP1, a p53-inducible gene, regulates p53-dependent apoptosis. *Mol Cell* 8:85–94.
35. Fiscella M, et al. (1997) Wip1, a novel human protein phosphatase that is induced in response to ionizing radiation in a p53-dependent manner. *Proc Natl Acad Sci USA* 94:6048–6053.
36. Kirsch DG, et al. (1999) Caspase-3-dependent cleavage of Bcl-2 promotes release of cytochrome c. *J Biol Chem* 274:21155–21161.
37. Bagci EZ, Vodovotz Y, Billiar TR, Ermentrout GB, Bahar I (2006) Bistability in apoptosis: roles of Bax, Bcl-2, and mitochondrial permeability transition pores. *Biophys J* 90:1546–1559.
38. Geske FJ, Lieberman R, Srtange R, Gerschenson LE (2001) Early stages of p53-induced apoptosis are reversible. *Cell Death Differ* 8:182–191.
39. Kitano H (2004) Cancer as a robust system: implications for anticancer therapy. *Nat Rev Cancer* 4:227–235.
40. Cory S, Adams JM (2002) The Bcl2 family: regulators of the cellular life-or-death switch. *Nat Rev Cancer* 2:647–656.
41. Schultz D, Ben Jacob E, Onuchic JN, Wolynes PG (2007) Molecular level stochastic model for competence cycles in Bacillus subtilis. *Proc Natl Acad Sci USA* 104:17582–17587.
42. Schultz D, Walczak AM, Onuchic JN, Wolynes PG (2008) Extinction and resurrection in gene networks. *Proc Natl Acad Sci USA* 105:19165–19170.
43. Lapidus S, Han B, Wang J (2008) Intrinsic noise, dissipation cost, and robustness of cellular networks: The underlying energy landscape of MAPK signal transduction. *Proc Natl Acad Sci USA* 105:6039–6044.
44. Lepzelter D, Kim KY, Wang J (2007) Dynamics and intrinsic statistical fluctuations of a gene switch. *J Phys Chem B* 111:10239–10247.
45. Kim KY, Wang J (2007) Potential energy landscape and robustness of a gene regulatory network: toggle switch. *PLoS Comput Biol* 3:e60.

Supporting information (SI)

"Cell fate decision mediated by p53 pulses"

Xiao-Peng Zhang, Feng Liu, Zhang Cheng, and Wei Wang

In this work, we aim at the p53 signaling network in untransformed mammalian cells, i.e., without genetic mutations in the involved factors of p53 response. We investigate the response of p53 signaling network to DNA damage in a population of 2000 cells. There are four modules in the model: a DNA repair module, an ataxia telangiectasia mutated (ATM) switch, the p53-Mdm2 oscillator and a cell fate decision module. Remarkably, we assume that p53 regulation of DNA repair is threshold-dependent, i.e., p53 promotes DNA repair when DNA damage is below a given threshold and otherwise suppresses DNA repair. In the following, we present the details of the model including equations and parameter values. The equations were solved numerically using a second-order Runge-Kutta algorithm with a time step $\Delta t = 0.01$, and the bifurcation diagrams are plotted using XPPAUT and Oscill 8.

Details of the Model

Stochastic Simulation of the Generation and Repair of DNA damage. Double-strand breaks (DSBs) are the predominant DNA lesions caused by ionizing radiation (IR). In mammalian cells, there are two major repair mechanisms for DSB repair: homologous recombination (HR) and nonhomologous end joining (NHEJ) [1, 2]. The NHEJ is the predominant pathway for DSB repair in mammalian cells, especially in G1 phase of the cell cycle [3]. There are two principal mechanisms for NHEJ: error-prone rejoining and precise ligation (error-free repair) [4]. The repair of IR-induced DNA damage is generally error-prone because IR destroys sequence information [4]. It has been proposed that p53 may control the fidelity of DSB repair by promoting precise repair but suppressing error-prone repair [1]. The fidelity of DSB repair reduces with increasing IR dose, and excessive DSBs may force normal NHEJ components to process DSBs aberrantly [5]. Therefore, we introduce the dose-dependent p53 regulation of DNA repair to the model, and assume that p53 promotes the DSB repair when the initial number of DSBs is below a threshold and otherwise suppresses the DSB repair. This threshold is set to 175, the mean number of DSBs produced at the radiation dose of $D_{\mathrm{IR}} = 5$ Gy.

Owing to stochasticity in the DNA repair process, we use the Monte Carlo method to simulate

the DNA repair dynamics. In the simulations, given the IR dose of y Gy, the initial number of DSBs in each cell is generated from a Poisson distribution with the mean of $35y$ [6], and the total number of DNA repair proteins is assumed to be 20 in each cell. We consider three states in the DSB repair process: intact DSB, DSB-protein complex (DSBC) and fixed DSB. For the sake of simplicity, the above three states are called state D, C and F, respectively. The numbers of DSBs in each state are represented by n_{D}, n_{C} and n_{F}, respectively. The schematic diagrams of DSB repair process are presented in Fig. S1. We use subscripts '1' and '2' to distinguish fast kinetics from slow kinetics [7]. The Monte Carlo algorithm for the repair dynamics is based on the transition probabilities between two neighboring states as follows:

$$\begin{aligned}
P_{D_1\to C_1} &= RP[k_{fb1} + k_{cross}(D_1 + D_2)]\Delta t \\
P_{D_2\to C_2} &= RP[k_{fb2} + k_{cross}(D_1 + D_2)]\Delta t \\
P_{C_1\to D_1} &= k_{rb1}\Delta t \\
P_{C_2\to D_2} &= k_{rb2}\Delta t \\
P_{C_1\to F_1} &= k_{fix1}\Delta t \\
P_{C_2\to F_2} &= k_{fix2}\Delta t.
\end{aligned} \tag{1}$$

In the above, all the ratios of the rates for the fast kinetics to those for the slow kinetic are chosen to be close to 10. It is also assumed that the binding of repair proteins to DSBs is much faster than other processes such as dissociation of repair proteins and the repair process. That is, the number of DSBCs is 20 when DSBs are more than repair proteins, while this number is equal to the number of DSBs when DSBs are fewer than repair proteins. We consider the p53 regulation of DNA repair, and the fixing rate of DNA repair should be p53-dependent. If $n_{\mathrm{D}} < 175$, the rates are described by

$$\begin{aligned}
k_{fix1} * (1 + \frac{[p53^*]}{1 + [p53^*]}), \\
k_{fix2} * (1 + \frac{[p53^*]}{1 + [p53^*]}).
\end{aligned} \tag{2}$$

If $n_{\mathrm{D}} \geq 175$, the rates are described by

$$\begin{aligned}
k_{fix1} * (1 - \frac{[p53^*]}{1 + [p53^*]}), \\
k_{fix2} * (1 - \frac{[p53^*]}{1 + [p53^*]}).
\end{aligned} \tag{3}$$

The Monte Carlo algorithm for the DBS repair dynamics at the IR dose of y Gy is presented in the following:

1. Generation of DSBs. Set t=0. The initial number of total DSBs $n_{\rm D}(0)$ is generated from a Poisson distribution with a mean value of 35y. The initial values for simple and complex DSB repair are taken as $n_{\rm D1}(0) = 0.7n_{\rm D}(0)$ and $n_{\rm D2}(0) = 0.3n_{\rm D}(0)$, respectively, while the numbers of DSBs in other states are set to zero, namely, $n_{\rm C1}(0) = n_{\rm C2}(0) = n_{\rm F1}(0) = n_{\rm F2}(0) = 0$. The total number of repair proteins $n_{\rm RP}$ is set to 20, and the number of free repair proteins is $n_{\rm RP}(0) = 20$.

2. Increasing time from t to $t = t + \triangle t$.

3. Update the states for each of the damages sites controlled by fast repair. For each damage locus i (with $1 \leq i \leq n_{\rm D1}(0)$), a random number r is generated from a uniform distribution between 0 and 1. If the damage at locus i is in state D, a transition to state C occurs if $0 \leq r < P_{D1\rightarrow C1}$, while it stays in state D if $P_{D1\rightarrow C1} \leq r \leq 1$. If the damage is in state C, a transition to state D occurs if $0 \leq r < P_{C1\rightarrow D1}$, or a transition to state F occurs if $P_{C1\rightarrow D1} \leq r < P_{C1\rightarrow D1} + P_{C1\rightarrow F1}$. If the damage is in state F, it always stays in state F (i.e., state F is absorbing). Set $n_{\rm RP} = n_{\rm RP} + 1$ if transition from state C to D or from state C to F occurs ; set $n_{\rm RP} = n_{\rm RP} - 1$ if transition from state D to C occurs; otherwise $n_{\rm RP}$ remains the same. After the last damage site has been updated, set the numbers of fast repaired breaks at time t in states D, C, and F to be $n_{\rm D1}$, $n_{\rm C1}$ and $n_{\rm F1}$, respectively.

4. Update the states for each of the damages sites controlled by slow repair. For each damage locus i (with $1 \leq i \leq n_{\rm D2}(0)$), a random number r is produced from a uniform distribution between 0 and 1. If the damage at locus i is in state D, a transition to state C occurs if $0 \leq r < P_{D2\rightarrow C2}$, while it stays in state D if $P_{D2\rightarrow C2} \leq r \leq 1$. If the damage is in state C, a transition to state D occurs if $0 \leq r \leq P_{C2\rightarrow D2}$, or a transition to state F occurs if $P_{C2\rightarrow D2} \leq r < P_{C2\rightarrow {\rm D}2} + P_{C2\rightarrow F2}$. If the damage is in state F, it always stays in state F (i.e., state F is absorbing). Set $n_{\rm RP} = n_{\rm RP} + 1$ if transition from state C to D or from state C to F occurs ; set $n_{\rm RP} = n_{\rm RP} - 1$ if transition from state D to C occurs; otherwise $n_{\rm RP}$ remains the same. After the last damage site has been updated, set the numbers of slow repaired breaks at time t in states D, C, and F to be $n_{\rm D2}$, $n_{\rm C2}$ and $n_{\rm F2}$, respectively.

5. Let $n_{\rm D}(t) = n_{\rm D1}(t) + n_{\rm D2}(t)$, $n_{\rm C}(t) = n_{\rm C1}(t) + n_{\rm C2}(t)$, and $n_{\rm F}(t) = n_{\rm F1}(t) + n_{\rm F2}(t)$.

6. Repeat steps 2-5 until all of the DSBs are effectively repaired, i.e., $n_{\rm D} \leq 2$.

Equations for the ATM Switch Module. Ataxia telangiectasia mutated (ATM) acts as a DSB detector and can be activated by DSBCs. The ATM switch module is composed of three

components: ATM dimer (ATM_2), inactive ATM monomer (ATM), and active ATM monomer (ATM^*) (Fig. S2). The dynamics of the ATM switch are characterized by ordinary differential equations (ODEs) as follows:

$$\begin{aligned} \frac{d[ATM_2]}{dt} &= k_{dim}[ATM]^2 - k_{undim}[ATM_2] && (4)\\ k_{1s} &= k_{1s0}[ATM^*]\frac{n_C}{n_C + j_{n_C}} \\ \frac{d[ATM^*]}{dt} &= k_{1s}\frac{[ATM]}{[ATM] + j_{1s}} - k_{2s}\frac{[ATM^*]}{[ATM^*] + j_{2s}} && (5)\\ [ATM] &= [ATM_{tot}] - 2[ATM_2] - [ATM^*] && (6) \end{aligned}$$

where $[ATM_2], [ATM]$ and $[ATM^*]$ are the concentrations of ATM dimers, inactive ATM monomers and active ATM monomers, respectively. In our model, the total concentration of ATM is assumed to be a constant, namely, $2[ATM_2] + [ATM] + [ATM^*] = [ATM_{tot}]$. The ATM monomers dimerize with a rate k_{dim}, and the ATM dimers disassociate with a rate k_{undim}. The rates of inactive ATM monomers activation and active monomers deactivation are k_{1s} and k_{2s}, respectively.

A positive feedback loop is significant for the activation of the ATM switch, i.e., the active ATM^* can promote the activation of inactive ATM through intermolecular autophosphorylation [8]. In addition, DSBCs can accelerate the activation of ATM^* [8], and k_{1s} is a function of the amounts of DSBC and ATM^*. Based on the positive feedback, the dynamics of ATM^* are characterized as a bistable switch, i.e., ATM^* level switches between two discrete 'on' and 'off' states, and this will send an on-off switching signal to the p53-Mdm2 oscillator.

Equations for the p53-Mdm2 Oscillator Module. The p53-Mdm2 oscillator can be initiated by the ATM switch. Two core proteins are involved in the p53-Mdm2 oscillator: p53 and Mdm2 (Fig. 2). Two forms of p53 in the nucleus are considered, inactive p53 and active $p53^*$, while the cytoplasmic p53 is not considered here. The Mdm2 in two compartments, $\mathrm{Mdm2_{nuc}}$ and $\mathrm{Mdm2_{cyt}}$, are involved, and they can shuttle between the nucleus and cytoplasm with rates k_i and k_o. Mdm2 acts as a ubiquitin ligase to target p53 for degradation by the proteasome. In the nucleus, inactive p53 is degraded rapidly by Mdm2 with a rate k_{d53}, while active $p53^*$ is degraded slowly with a rate k_{d53^*}. As a phosphorylation kinase, ATM^* induces the activation of p53 with a rate k_{ac}, and $p53^*$ can be deactivated with a basal rate k_{in}. For simplicity, we assume that both the degradation rate of Mdm2 and activation rate of p53 increase linearly with the ATM^* level.

Remarkably, two coupled positive and negative feedback loops are considered in the p53-Mdm2 oscillator module (Fig. 2). One is the negative feedback loop between p53* and $\mathrm{Mdm2_{nuc}}$: p53* promotes production of $\mathrm{Mdm2_{cyt}}$, which then enters the nucleus to targets p53 for degradation. The other is a positive feedback loop between p53* and $\mathrm{Mdm2_{cyt}}$: p53* induces *Mdm2* to synthesize $\mathrm{Mdm2_{cyt}}$, which promotes the translation of *p53* mRNA to produce inactive p53 [9]. It can be expected that robust and reliable p53 oscillations can be accomplished through a combination of negative and positive feedback loops rather than a single negative feedback loop with a time delay [10]. The corresponding dynamical equations for this module are presented as follows:

$$k_{d2} = k_{d21}(1 + [ATM^*]) \tag{7}$$

$$k_{ac} = k_{ac0}(1 + [ATM^*]) \tag{8}$$

$$k_{d53^*} = k_{d531} + k_{d532}G([Mdm2_{nuc}], \theta, J_{d53^*}/[p53^*, J_{d53^*}/[p53^*]) \tag{9}$$

$$k_{d53} = k_{d531} + k_{d532}G([Mdm2_{nuc}], \theta, J_{d53}/[p53], J_{d53}/[p53]), \tag{10}$$

where the Goldbeter-Koshland function, G, is defined as:

$$G(u, v, x, y) = \frac{2uy}{v - u + vx + uy + \sqrt{(v - u + vx + uy)^2 - 4(v - u)uy}}.$$

$$\frac{d[p53]}{dt} = k_{s531} + k_{s532}\frac{[Mdm2_{cyt}]^4}{j_{s53}^4 + [Mdm2_{cyt}]^4} + k_{in}[p53^*] - k_{ac}[p53] - k_{d53}[p53] \tag{11}$$

$$\frac{d[p53^*]}{dt} = k_{ac}[p53] - k_{in}[p53^*] - k_{d53^*}[p53^*] \tag{12}$$

$$\frac{d[Mdm2_{cyt}]}{dt} = k_{s21} + k_{s22}\frac{[p53^*]^4}{j_{s2}^4 + [p53^*]^4} - k_i[Mdm2_{cyt}] + k_o[Mdm2_{nuc}] - k_{d22}[Mdm2_{cyt}] \tag{13}$$

$$\frac{d[Mdm2_{nuc}]}{dt} = k_i[Mdm2_{cyt}] - k_o[Mdm2_{nuc}] - k_{d2}[Mdm2_{nuc}]. \tag{14}$$

Equations for the Cell Fate Decision Module. Many factors, such as stress signals, co-factors and post-translational modifications, can affect the stability and selectivity of p53 in target gene expression [11–13]. Especially, here two forms of active p53* are distinguished: p53 arrester and p53 killer (Fig. 3). p53 arrester is the primarily phosphorylated p53 on Ser15, while p53 killer refers to further phosphorylated p53, such as phosphorylated p53 on Ser46. p53 arrester regulates three target genes: *Wip1*, *p53DINP1* and *p21*, while p53 killer regulates two target genes: *p53DINP1* and *p53AIP1*. Two other apoptotic components are also included, namely, cytochrome c (CytoC) and Caspase 3 (Casp3) (Fig. 3).

The two forms of p53* perform different functions in cell fate decision. p53 arrester-induced p53DINP1 promotes phosphorylation of p53 on Ser46, i.e., formation of p53 killer, while Wip1 promotes reversion of p53 killer to p53 arrester. p53 arrester induces cell cycle arrest through activating CDK inhibitor p21, while p53 killer induces pro-apoptotic genes such as *p53AIP1*. Over-expression of *p53AIP1* can induce release of CytoC from mitochondria and activation of apoptosis executioner Casp3. Compared with the model by Zhang *et al.* [13], here two forms of p53 are considered by ignoring the intermediate one, and the complete process of apoptosis is characterized by including the ultimate activation of Casp3, which is the most reliable marker of apoptosis.

Here apoptosis is modeled as a bistable switch [14–16]. The 'life steady state' means no considerable caspases are activated, whereas 'death steady state' refers to almost full activation of caspases leading to apoptosis. In addition, we consider a positive feedback loop between CytoC and Casp3 (see Fig. 3). The release of CytoC leads to activation of Casp3, which in turn cleaves the inhibitors of p53AIP1 (such as Bcl-2 and Bcl-xL) to enhance release of CytoC [17, 18]. Therefore, a bistable switch can be constructed based on this positive feedback loop. Senescence due to permanent cell cycle arrest is not considered here. Moreover, although many inhibitors and enablers of apoptosis in the Bcl-2 family, like Bcl-2, Bcl-xL, Bax and Puma, are important to regulation of cell fate decision [19, 20], they are not considered here for the sake of simplicity. The detailed equations for this module are presented as follows:

$$\frac{d[p53\ killer]}{dt} = [p53DINP1]\frac{[p53\ arrester]}{j_{arrester}+[p53\ arrester]} - [Wip1]\frac{[p53\ killer]}{j_{killer}+[p53\ killer]} \quad (15)$$

$$[p53\ arrester] = [p53^*] - [p53\ killer] \quad (16)$$

$$\frac{d[Wip1]}{dt} = k_{sWip11} + k_{sWip12}\frac{[p53\ arrester]^3}{j_{sWip1}^3+[p53\ arrester]^3} - k_{dWip1}[Wip1] \quad (17)$$

$$\frac{d[p21]}{dt} = k_{sp211} + k_{sp212}\frac{[p53\ arrester]^3}{j_{sp21}^3+[p53\ arrester]^3} - k_{dp21}[p21] \quad (18)$$

$$\frac{d[p53DINP1]}{dt} = k_{sDINP11} + k_{sDINP12}\frac{[p53\ arrester]^3}{j_{sDINP11}^3+[p53\ arrester]^3} + k_{sDINP13}\frac{[p53\ killer]^3}{j_{sDINP12}^3+[p53\ killer]^3} - k_{dDINP1}[p53DINP1] \quad (19)$$

$$\frac{d[p53AIP1]}{dt} = k_{sAIP11} + k_{sAIP12}\frac{[p53\ killer]^3}{j_{sAIP1}^3+[p53\ killer]^3} - k_{dAIP1}[p53AIP1] \quad (20)$$

$$\frac{d[CytoC]}{dt} = k_{sCytoC}[p53AIP1]\frac{[Casp3]^4}{j_{Casp3}^4 + [Casp3]^4}[CytoC_{mito}] - k_{dCytoC}[CytoC] \quad (21)$$

$$\frac{d[Casp3]}{dt} = k_{sCasp31} + k_{sCasp32}\frac{[CytoC]^4}{j_{CytoC}^4 + [CytoC]^4} - k_{dCasp3}[Casp3] \quad (22)$$

$$[CytoC_{mito}] = [CytoC_{tot}] - [CytoC] \quad (23)$$

Details of the Results

The Connection Between Repair Time and Radiation Dose. Repair time is defined as the time taken for the number of DSBCs to reduce below two, i.e., $n_C \leq 2$. For a population of 2000 cells, the stochasticity in DNA repair is characterized in two aspects: the distribution of repair time and the mean repair time. Figure S3 shows the distribution of the repair time for the population at IR doses from 3 Gy to 7 Gy for the cases with and without p53 regulation of DNA repair. For the case without p53 regulation, the mean repair time increases monotonically with $D_{\rm IR}$, and the histograms shift rightward with increasing $D_{\rm IR}$ and are always unimodal (see the black lines).

Given the p53 regulation of DNA repair, the histograms are unimodal at low and high IR doses, while the histograms are bimodal around $D_{\rm IR}$=5 Gy. At low doses, p53 promotes the DNA repair with high fidelity, and thus the histograms for the cases with p53 regulation shift leftward (see the the first two histograms with red color in Fig.S3). At high doses, p53 suppresses the DNA repair, and the histograms shift rightward and become more widespread (see the last two histograms with red color in Fig. S3).

Interestingly, for the dose around $D_{\rm IR} = 5$ Gy, the histograms are bimodal (see the intermediate three histograms with red color in Fig. S3). These particular results originate from the threshold-dependent p53 regulation of DNA repair. p53 promotes the DNA repair when the initial number of DSBs is smaller than 175 but otherwise suppresses the DNA repair. That is, compared with the cases without p53 regulation, the repair time for some cells decreases due to the promotion of the repair and that for the others increases due to the suppression of the repair. As a result, the distribution of repair time is bimodal, composed of two small peaks.

Figure S4 displays the mean repair time for two cases. Clearly, the mean repair time for the case with p53 regulation is larger than that for the case without p53 regulation if $D_{IR} > 5$ Gy. This further identifies the dual role of p53 in DNA repair, i.e. p53 promotes DNA repair at low

IR doses but suppresses DNA repair at high doses.

The detailed dynamics of the ATM switch. As a detector of DSBs, ATM exhibits a switch-like behavior and plays a controlling role in setting a threshold level of DNA damage. Figure S5 displays the steady-state level of ATM* versus the number of DSBCs, $n_{\rm C}$. ATM activation starts with $n_{\rm C} = 5$, whereas ATM deactivation occurs when $n_{\rm C} = 2$, which ensures that DNA damage is effectively repaired (see the inset). Indeed, ATM is extremely sensitive to DNA damage; a $0.1 - 0.2$ Gy dose of IR can activate ATM. The simulation results are consistent with experimental observations, where 0.1-Gy IR can be detected by ATM and ATM activation becomes maximal at 0.5-Gy IR [8]. Figure S6 shows the time course of ATM* level for three individual cells at various IR doses. Upon IR, ATM is activated very rapidly, and ATM* level remains maximal over the first 800 min. Once $n_{\rm C}$ falls below a threshold (see Fig. S5), the ATM* level decays to zero much faster than $n_{\rm C}$. This sharp, step-like response of ATM* results from the positive feedback involved in ATM phosphorylation [8]. Clearly, the duration of active ATM prolongs with increased IR dose and is determined by the repair time. In addition, owing to stochasticity in DNA repair, cells exhibit considerable variability in the time courses of the ATM switch for IR with certain dose.

Parameter Dependence of P53 Oscillation. We change the values of parameters contained in this module by 20% around the control parameter set (the blue star) to check the robustness of p53 oscillation. The p53 level still exhibits periodic oscillations, and the variations in the period and amplitude of p53 pulses are constrained within 10% for most of the parameters (see Fig. S7). Especially, the period and amplitude of the oscillation is relatively sensitive to the synthesis and degradation rates of p53 and Mdm2. Our simulations also show that p53 oscillation will disappear if the basal induction rate of Mdm2 is increased 3-fold or the basal transcription rate of p53 is increased 4-fold (Fig. S8). This is consistent with the experimental observation that p53 oscillations were not observed in cells containing high-level Mdm2 as observed with a single nucleotide polymorphism in the *Mdm2* gene, which may contribute to tumorigenesis in those cells [21]. Therefore, too high level of p53 or Mdm2 fails to generate sustained oscillation, and only matched levels of p53 and Mdm2 generate the oscillation.

Damped Oscillation in Cell Population. It has been reported that p53 level exhibits damped oscillation at the population level upon IR [22]. Figure S9 shows the averaged p53 level over 2000 cells at IR doses of 1, 3 and 5 Gy. At the low dose of $D_{\rm IR}$ =1 Gy, the typical property

of the damped oscillation is observable, i.e., the p53 level exhibits decreasing amplitude in its second and third pulses. At the moderate dose of D_{IR}=3 Gy, the first two pulses have the same amplitude, but the amplitude drops since the third pulse. At D_{IR} = 5 Gy, the amplitude of pulses decays only after the fourth pulse. Here the damped oscillation of p53 level is consistent with the distribution of the pulse number in Fig. 7*D*. At D_{IR}=1 Gy, the first pulse of p53 level exists in almost all cells, while the second and third pulses only appear in some cells. Thus, the mean p53 level shows damped oscillation. When increasing D_{IR}, all the cells share the first two or three pulses, and thus the amplitude of p53 level decays after the first two or three pulses.

Regulation of the Apoptotic Switch by p53AIP1. The ultimate fate of cells is decided by the apoptotic switch, which is controlled by p53 pulses. As a target gene of p53, *p53AIP1* can be induced only by pulses of p53 killer, and this is crucial for the subsequent initiation of the apoptotic switch. Fig. S10 shows the bifurcation diagram of [Casp3] versus [p53AIP1]. The steady state of [Casp3] dose show the property typical of a bistable switch, i.e., a high level of p53AIP1 (about 0.7) turns on the switch with full activation of Casp3, and a rather low level of p53AIP1 (about 0.006) turns off the switch. According to our model, the basal level of p53AIP1 is about 0.08, which is much higher than the deactivated threshold (0.006). Thus, the apoptotic switch becomes irreversible after it is turned on. Our modeling is consistent with previous experimental observation that apoptosis is really irreversible after 'the point of no return'.

Integration of the levels of p53AIP1 and Casp3 over p53 pulses. In Fig. S11, two distinct cell fates are presented at the same radiation dose of D_{IR}=5 Gy. It is shown that the levels of p53AIP1 and p53 killer are gradually integrated over the pulses of p53 helper relying on the extent of DNA damage. If DNA damage is quickly repaired, the integration of p53AIP1 is not sufficient to drive the executioner of apoptosis, Casp3, to exceed the certain threshold (the left column). Thus, the cell can recover to normal growth after transient p53 pulses. However, when DNA damage is severe, the level of p53AIP1 accumulates to a sufficiently high level and oscillates there owing to sustained p53 pulses (the right column). As a result, Casp3 is irreversibly activated, and apoptosis ensues.

Annotations on the Model. For the sake of simplicity, we did not consider senescence due to permanent cell cycle arrest [23]. We omitted some other factors related to apoptosis, like Bcl-2, Apaf1, Bax and Puma *etc.* [24]. Although these factors are important to the regulation

of apoptosis under some conditions, there is no direct evidence that they are target genes of p53 killer. Moreover, another important transcription factor E2F1 is not explicitly included in our model since its role is to enhance the apoptosis cooperating with p53 [25]. Nevertheless, its influence is partially implicated in our model through tuning parameter values. In addition, we did not consider a variety of p53 cofactors such as ASSP1, ASSP2, HIPK2 and Hzf [26], which may be important to the promoter selectivity of p53. But our model can be easily extended to include these cofactors since it represents a general framework for cell fate decision by p53 pulses. Finally, note that the stochasticty is only involved in the DNA repair module, and intrinsic noise from gene expression in the other modules is not considered. Therefore, it is intriguing to investigate the effects of intrinsic noise in the p53 network on cell fate decision.

Note that permanent p53 oscillations can occur in the transformed MCF7 cells [27], which are deficient in DNA repair and inducing apoptosis [28–30]. Considering the effects of DNA repair, our model can explain the the presence of p53 permanent oscillations in the transformed cells. We propose that the number of p53 pulses can be used to distinguish cell survival from apoptosis. Thus, our proposal that cell fate can be determined by counting the number of p53 pulses represents a plausible mechanism. Moreover, p53 level can admit various behaviors, such as monostablity, oscillations and bistability at different parameter settings in our model. It is easy to modify parameter values to accommodate new experimental observations in our integrated model.

[1] Sengupta S, Harris CC (2005) p53: traffic cop at the crossroads of DNA repair and recombination. *Nat Rev Mol Cell Biol* 6:44-55.

[2] Gatz SA, Wiesmuller L (2006) p53 in recombination and repair. *Cell Death Differ* 13:1003-1016.

[3] Burma S, Chen BPC, Chen DJ (2006) Role of non-homologous end joining (NHEJ) in maintaining genomic integrity. *DNA Repair* 5:1042-1048.

[4] Dahm-Daphi J, *et al.* (2005) Nonhomologous end-joining of site-specific but not of radiation-induced DNA double-strand breaks is reduced in the presence of wild-type p53. *Oncogene* 24:1663-1672.

[5] Brady N, Gaymes TJ, Cheung M, Mufti GJ, Rassool FV (2003) Increased error-prone NHEJ activity in myeloid leukemias is associated with DNA damage at sites that recruit key nonhomologous end-joining proteins. *Cancer Res* 63:1798-1805.

[6] Ma L, *et al.* (2005) A plausible model for the digital response of p53 to DNA damage. *Proc Natl Acad Sci USA* 102:14266-14271.

[7] Stewart RD (2001) Two-lesion kinetic model of double-strand break rejoining and cell killing. *Radiat Res* 156:365-378.

[8] Bakkenist CJ, Kastan MB (2003) DNA damage activates ATM through intermolecular autophosphorylation and dimer dissociation. *Nature* 421:499-506.

[9] Yin Y, Stephen CW, Luciani MG, Fahraeus R (2002) p53 stability and activity is regulated by Mdm2-mediated induction of alternative p53 translation products. *Nat Cell Biol* 4:462-467

[10] Pomerening JR, Kim SY, Ferrell JE Jr (2005) Systems-Level Dissection of the Cell-Cycle Oscillator: Bypassing Positive Feedback Produces Damped Oscillations. *Cell* 122:565-578.

[11] Vousden KH, Lu X (2002) Live or let die: the cell's response to p53. *Nat Rev Cancer* 2:594-604.

[12] Oren M (2003) Decision making by p53: life, death and cancer. *Cell Death Differ* 10:431-442.

[13] Zhang T, Brazhnik P, Tyson JJ (2007) Exploring mechanisms of the DNA-damage response: p53 pulses and their possible relevance to apoptosis. Cell Cycle 6:85-94.

[14] Bagci EZ, Vodovotz Y, Billiar TR, Ermentrout GB, Bahar I (2006) Bistability in apoptosis: roles of P53AIP1, Bcl-2, and mitochondrial permeability transition pores. *Biophys J* 90:1546-1559.

[15] Eissing T, *el al.* (2004) Bistability analyses of a caspase activation model for receptor-induced apoptosis. *J Biol Chem* 279:36892-36897.

[16] Legewie S, Blüthgen N, Herzel H (2006) Mathematical Modeling identifies inhibitors of apoptosis as mediators of positive feedback and bistability. *PLoS Compt Biol* 2:e120.

[17] Kim Y-M, Kim T-H, Seol D-W, Talanian RV, Billiar TR (1998) Nitric oxide suppression of apoptosis occurs in association with an inhibition of Bcl-2 cleavage and cytochrome c release. *J Biol Chem* 273:31437-31441.

[18] Kirsch DG, et al. (1999) Caspase-3-dependent cleavage of Bcl-2 promotes release of cytochrome c. *J Biol Chem* 274:21155-21161.

[19] Adams JM, Cory S (2006) The Bcl-2 apoptotic switch in cancer development and therapy. *Oncogene* 26:1324-1337.

[20] Youle RJ, Strasser A (2008) The BCL-2 protein family: opposing activities that mediate cell death. *Nat Rev Mol Cell Biol* 9:47-59.

[21] Hu W, et al. (2007) A single nucleotide polymorphism in the Mdm2 gene disrupts the oscillation of p53 and Mdm2 levels in cells. *Cancer Res* 67:2757-2765.

[22] Lev Bar-Or R, *et al.* (2000) Generation of oscillations by the p53-Mdm2 feedback loop: A theoretical and experimental study. *Proc Natl Acad Sci USA* 97:11250-11255.

[23] Campisi J, d'Adda di Fagagna F (2007) Cellular senescence: when bad things happen to good cells. *Nat Rev Mol Cell Biol* 8(9):729-740.

[24] Cory S, Adams JM (2002) The Bcl2 family: regulators of the cellular life-or-death switch. *Nat Rev Cancer* 2:647-656.

[25] Iaquinta PJ, Lees JA (2007) Life and death decisions by the E2F transcription factors. *Curr Opin Cell Biol* 19:649-657.

[26] Murray-Zmijewski F, Slee, EA, Lu X (2008) A complex barcode underlies the heterogeneous response of p53 to stress. *Nat Rev Mol Cell Biol* 9:702-712.

[27] Geva-Zatorsky N, *et al.* (2006) Oscillations and variability in the p53 system. *Mol Syst Biol* 2:2006.0033

[28] Blanc C, *et al.* (2000) Caspase-3 is essential for procaspase-9 processing and cisplatin-induced apoptosis of MCF-7 breast cancer cells. *Cancer Res* 60:4386-4390.

[29] Tyson JJ (2006) Another turn for p53. *Mol Syst Biol* 2:2006.0032.

[30] Francisco DC, *et al.* (2008) Induction and processing of complex DNA damage in human breast cancer cells MCF-7 and nonmalignant MCF-10A cells. *Free Radic Biol Med* 44:558-569.

Figure legends

Fig. S1: Schematic illustration of the generation and repair of DSBs. (A) DSB repair dynamics are characterized as a three-state process: DSB, DSB-protein complex and fixed DSB, and p53 promotes the repair of slightly damaged cells but suppresses the repair of irreparably damaged cells. (B) The two-lesion kinetic model of DNA repair. The model contains two parallel repair pathways with distinct reaction rates corresponding to fast and slow repair. The fast and slow kinetics refer to repair of simple and complex DSBs, respectively. D, C and F represent intact DSB, DSBC, and fixed DSB, respectively. Subscripts '1' and '2' are used to distinguish fast kinetics from slow kinetics.

Fig. S2: Illustration of the ATM switch. ATM predominantly exists as a dimer in unstressed cells. After DNA damage, intermolecular autophosphorylation occurs, and ATM dimers dissociate into active monomers. Here active ATM monomers can promote the formation of themselves, and the process is stimulated by DSBCs.

Fig. S3: Histogram of repair time for 2000 cells. The cell count versus the repair time is plotted for for the case with and without p53 regulation (red and black lines, respectively) at IR doses of 3, 4, 4.5, 5, 5.5, 6 and 7 Gy (from top to bottom).

Fig. S4: Mean repair time vs D_{IR} for the case with p53 regulation (red line) and without p53 regulation (black line). The mean repair time is obtained by averaging over 2000 individual cells.

Fig. S5: Bifurcation diagram of ATM* level vs n_{c}. Based on the positive feedback loop in the activation of ATM through intermolecular phosphorylation stimulated by DSBCs, ATM is modeled as a bistable switch. The switch is turned on with n_{C}=5, while it is turned off with n_{C}=2 (see the inset).

Fig. S6: Time courses of ATM* level for three individual cells at D_{IR}=4, 5, 6 Gy. On average, the duration of the switch in the 'ON' state prolongs with increasing D_{IR}. For certain D_{IR}, the duration displays considerable variability among three individual cells. The dotted lines indicates the threshold time for cell fate decision.

Fig. S7: Parameter sensitivity of the p53 oscillation. We show the dependence of the period and amplitude of p53 pulse on the parameter fluctuation. Here we change the values of parameters contained in this module by 20% around the control parameter set to check the robustness of p53 oscillation.

Fig. S8: Disappearance of p53 oscillation by increasing the basel transcription rate of p53 (k_{s531}) 4-fold, and that of Mdm2 (k_{s21}) 3-fold, respectively, at D_{IR}= 5 Gy. (A) p53 dynamics in three individual cells with $k_{s531} = 0.075$; (B) p53 dynamics in three individual cells with $k_{s21} = 0.016$.

Fig. S9: Damped oscillation of the mean p53 level averaged over a population of 2000 cells at D_{IR}= 1, 3 and 5 Gy. At low IR doses, typical properties of damped oscillation are observable. At D_{IR}= 3 and 5 Gy, the amplitudes decay in the last three pulses, while the first several pulses keep the same amplitude.

Fig. S10: Bifurcation diagram of Caspase 3 vs p53AIP1. The apoptotic switch is initiated by p53AIP1 with a level above a threshold (see the blue arrow), while it is turned off by p53AIP1 with a level close to zero (0.006). The resting state of p53AIP1 is about 0.08 (see the red arrow). That is, once the switch is turned on, it can remain in the 'ON' state even after the level of p53AIP1 drops to the resting state. Thus, the apoptotic switch becomes irreversible.

Fig. S11 : Time courses of the levels of p53 helper, p53 killer, p53AIP1 and Casp3 in two individual cells at D_{IR}=5 Gy. Two cells show distinct cell fates due to variability in the initial number of DSBs and the repair dynamics.

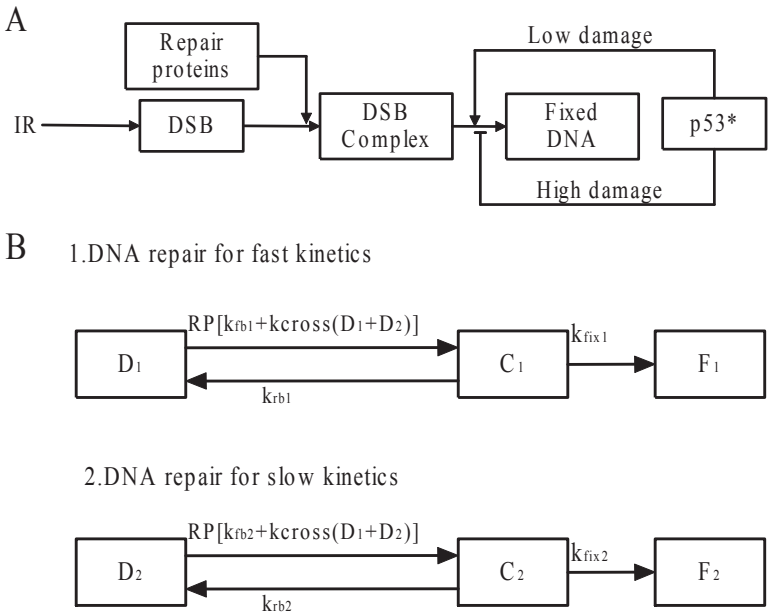
A
Repair proteins
IR
DSB
DSB Complex
Fixed DNA
p53*
Low damage
High damage
B
1.DNA repair for fast kinetics
RP[kfb1+kcross(D1+D2)]
D1
C1
F1
krb1
kfix1
2.DNA repair for slow kinetics
RP[kfb2+kcross(D1+D2)]
D2
C2
F2
krb2
kfix2

Fig.S1

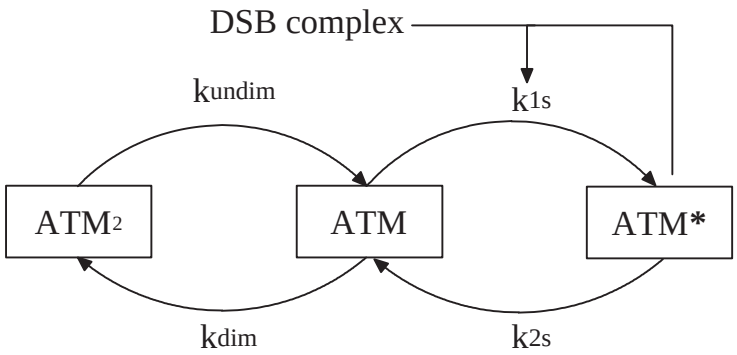
DSB complex
kundim
k1s
ATM2
ATM
ATM*
kdim
k2s

Fig.S2

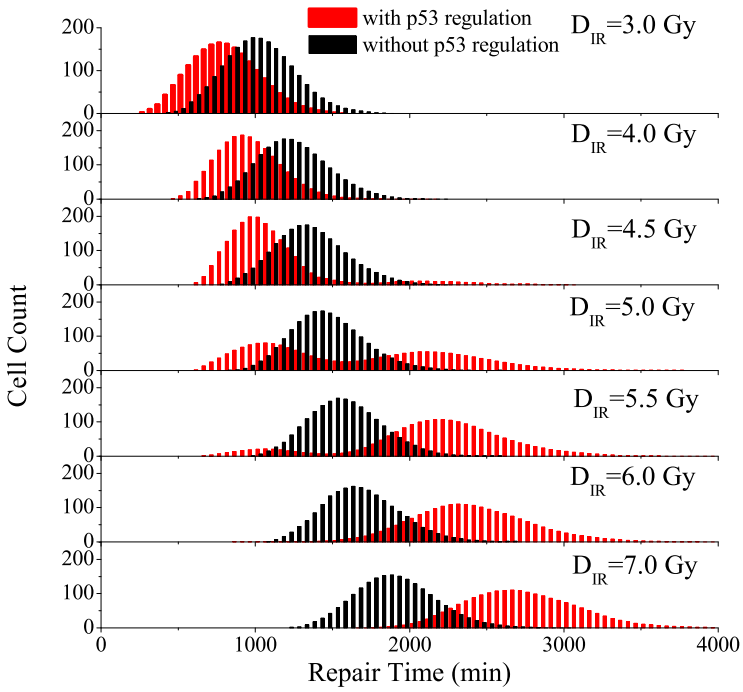
with p53 regulation
without p53 regulation
D_IR=3.0 Gy
D_IR=4.0 Gy
D_IR=4.5 Gy
D_IR=5.0 Gy
D_IR=5.5 Gy
D_IR=6.0 Gy
D_IR=7.0 Gy
Cell Count
Repair Time (min)
0
100
200
1000
2000
3000
4000

Fig.S3

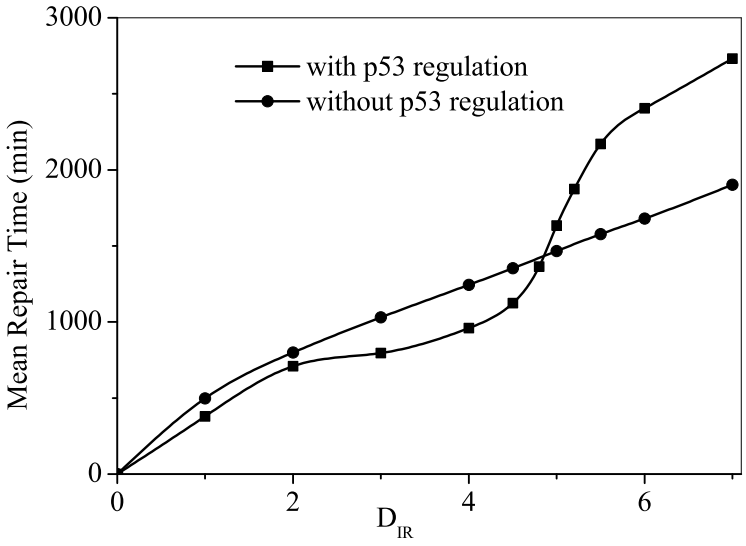
with p53 regulation
without p53 regulation
Mean Repair Time (min)
D_IR
0
1000
2000
3000
2
4
6

Fig.S4

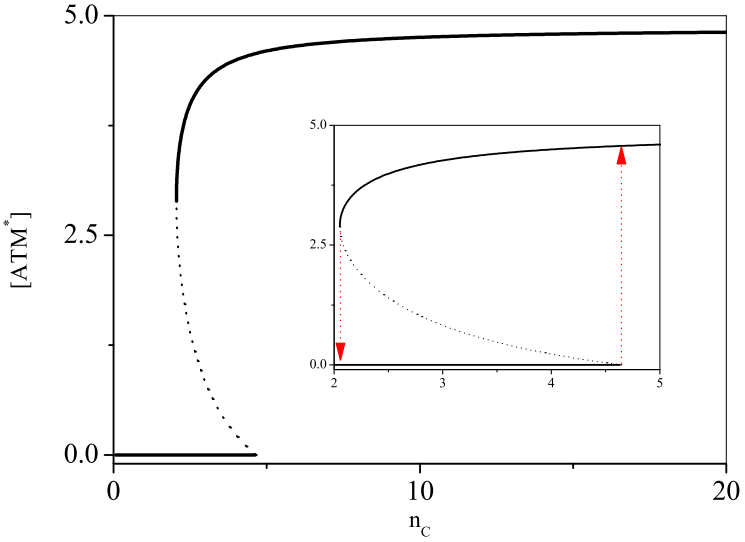
5.0
2.5
0.0
[ATM*]
0
10
20
n_C
5.0
2.5
0.0
2
3
4
5

Fig.S5

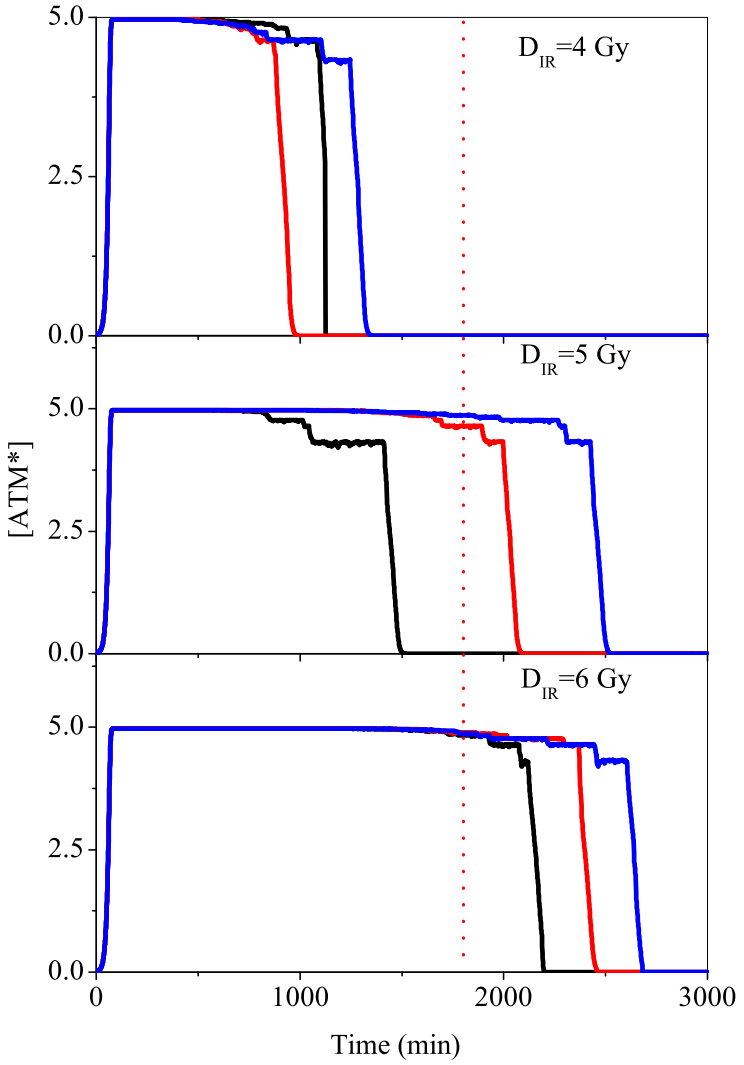
D_IR=4 Gy
D_IR=5 Gy
D_IR=6 Gy
[ATM*]
5.0
2.5
0.0
0
1000
2000
3000
Time (min)

Fig.S6

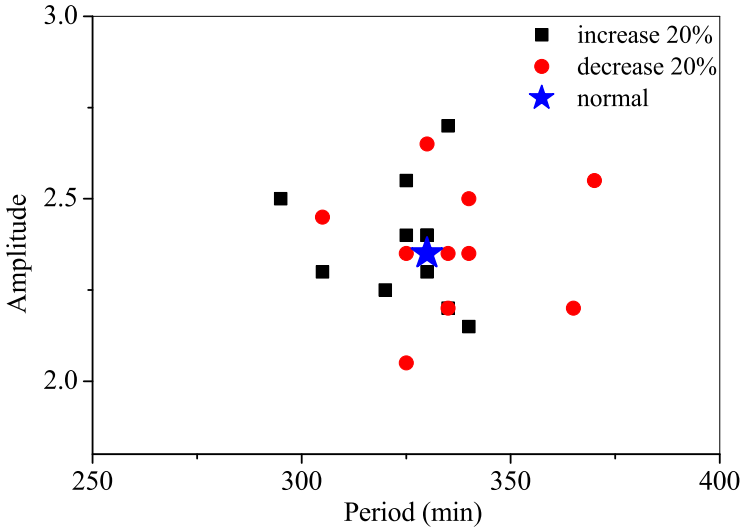
3.0
2.5
2.0
Amplitude
250
300
350
400
Period (min)
increase 20%
decrease 20%
normal

Fig.S7

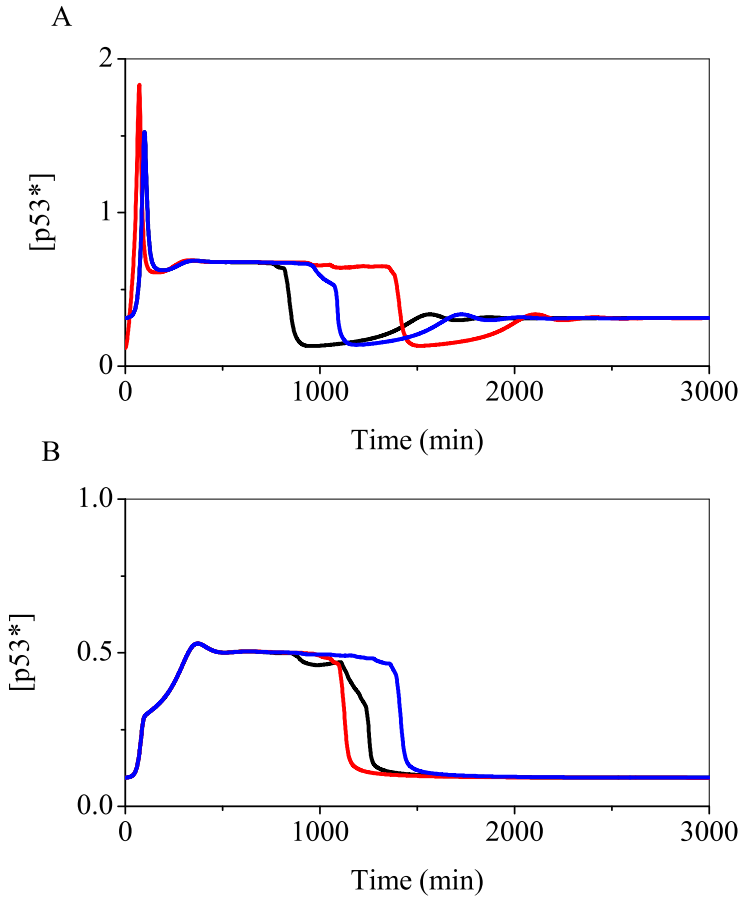
A
2
1
0
[p53*]
0
1000
2000
3000
Time (min)
B
1.0
0.5
0.0
[p53*]
0
1000
2000
3000
Time (min)

Fig.S8

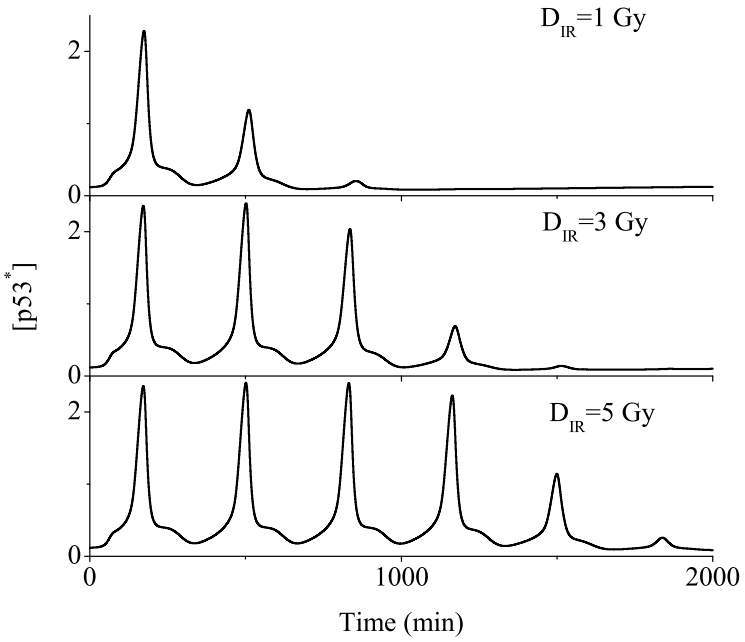

Fig.S9

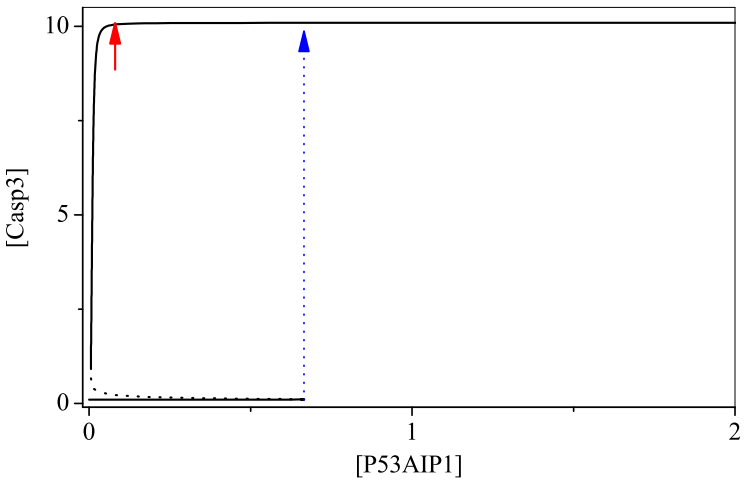

Fig.S10

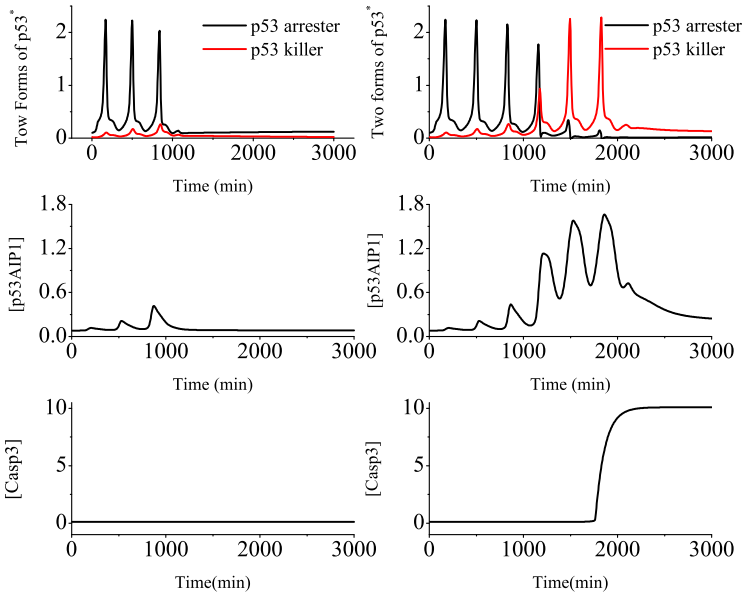
Tow Forms of p53*
p53 arrester
p53 killer
Time (min)
Two forms of p53*
p53 arrester
p53 killer
Time (min)
[p53AIP1]
Time (min)
[p53AIP1]
Time (min)
[Casp3]
Time(min)
[Casp3]
Time(min)

Fig.S11

TABLE I: Parameters for the whole model

Rate Constant	Description	Value
RPT	Number of repair proteins	20
k_{fb1}	Association rate of repair proteins in fast kinetics	2
k_{fb2}	Association rate of repair proteins in slow kinetics	0.2
k_{rb1}	Dissociation rate of repair proteins in fast kinetics	0.5
k_{rb2}	Dissociation rate of repair proteins in slow kinetics	0.05
k_{fix1}	DSB ligation rate in fast kinetics	0.03
k_{fix2}	DSB ligation rate in slow kinetics	0.003
k_{cross}	DSB binary mismatch rate	0.001
k_{dim}	ATM dimerization rate	5
k_{undim}	ATM undimerization rate	1
k_{1s0}	Basal activation rate of ATM	1.5
k_{2s}	ATM inactivation rate	0.8
j_{1s}	Michaelis constant of ATM activation	1
j_{2s}	Michaelis constant of ATM^* inactivation	2.5
j_{nC}	Threshold number of DSBC for ATM activation	4
ATM_{tot}	the total concentration of all forms of ATM	5
k_{s531}	Basal induction rate of p53	0.0016
k_{s532}	Mdm2-dependent production rate of p53	0.08
k_{d531}	Basal degradation rate of p53	0.0016
k_{d532}	Mdm2-dependent degradation rate of p53	0.08
θ	Threshold concentration for Mdm2-dependent p53 degradation	0.83
J_{d53^*}	Threshold concentration of p53* for Mdm2-dependent degradation	0.1
J_{d53}	Threshold concentration of p53 for Mdm2-dependent degradation	0.01
k_{d21}	Basal degradation rate of $Mdm2_{nuc}$	0.0013
k_{d22}	Degradation rate of $Mdm2_{cyt}$	0.0013
k_{s21}	Basal induction rate of $Mdm2_{cyt}$	0.004
k_{s22}	p53-dependent production rate of Mdm2	0.11
j_{s53}	threshold concentration of Mdm2-dependent p53 production	0.45
j_{s2}	Michaelis constant of p53-dependent Mdm2 production	0.92
k_i	Nuclear import rate of $Mdm2_{cyt}$	0.01
k_o	Nuclear export rate of $Mdm2_{nuc}$	0.0013
k_{ac}	Activation rate of $p53$	0.026
k_{in}	Inactivation rate of $p53^*$	0.0013

k_{sWip11}	Basal induction rate of $Wip1$	0.00054
k_{sWip12}	$p53$ *arrester* dependent production rate of $Wip1$	0.04
j_{sWip1}	Michaelis constant of $p53$ *arrester* dependent $Wip1$ production	1.8
k_{dWip1}	Degradation rate of $Wip1$	0.001
k_{sp211}	Basal induction rate of $p21$	0.0001
k_{sp212}	$p53$ *arrester* dependent production rate of $p21$	0.135
j_{sp21}	Michaelis constant of $p53$ *arrester* dependent $p21$ production	2
k_{dp211}	Degradation rate of $p21$	0.0054
$k_{sDINP11}$	Basal induction rate of $p53DINP1$	0.000054
$k_{sDINP12}$	$p53$ *arrester* dependent production rate of $p53DINP1$	0.0027
$k_{sDINP13}$	$p53$ *killer* dependent production rate of $p53DINP1$	0.135
$j_{sDINP11}$	Michaelis constant of $p53$ *arrester* dependent $p53DINP1$ production	0.4
j_{DINP12}	Michaelis constant of $p53$ *killer* dependent $p53DINP1$ production	0.5
k_{dDINP1}	Degradation rate of $p53DINP1$	0.00135
k_{sAIP11}	Basal induction rate of $p53AIP1$	0.0011
k_{sAIP12}	$p53$ *killer* dependent production rate of $p53AIP1$	0.027
j_{sAIP1}	Michaelis constant of $p53$ *killer* dependent $p53AIP1$ production	0.3
k_{dAIP1}	Degradation rate of $p53AIP1$	0.0135
k_{sCytoC}	P53AIP1 dependent cytochrome c activation rate	0.1
k_{dCytoC}	Inactivation rate of cytochrome c	0.005
$k_{sCasp31}$	Basal induction rate of Caspase 3	0.001
$k_{sCasp32}$	cytochrome c dependent production rate of Caspase 3	0.1
k_{dCasp3}	Degradation rate of Caspase 3	0.01
j_{CytoC}	Michaelis constant of Caspase 3 dependent cytochrome c production	0.3
j_{Casp3}	Michaelis constant of cytochrome c dependent Caspase 3 production	0.3
$CytoCtot$	Total concentration of cytochrome c	3